CONSERVATION AND VARIATIONS OF BIMODAL *HoxD* GENE REGULATION DURING TETRAPOD LIMB DEVELOPMENT

Nayuta Yakushiji-Kaminatsui[1], Lucille Lopez-Delisle[1,ɜ], Christopher Chase Bolt[1,ɜ], Guillaume Andrey[1,∞], Leonardo Beccari[2] and Denis Duboule[1,2,*]

[1]School of Life Sciences, Federal Institute of Technology, Lausanne, 1015 Lausanne, Switzerland, [2]Department of Genetics and Evolution, University of Geneva, 1211 Geneva 4, Switzerland.

[∞]Present address: Max Planck Institute for Molecular Genetics, RG Development & Disease, 14195 Berlin, Germany,

[ɜ]These authors contributed equally.

*Corresponding author: Denis.Duboule@epfl.ch

Keywords: Forelimb, hindlimb, genome topology, TADs, Polycomb, tetrapod evolution, enhancers

Short title: Comparative regulation of *Hoxd* genes during tetrapod limb development

ABSTRACT

In all tetrapods examined thus far, the development and patterning of limbs require the activation of gene members of the *HoxD* cluster. In mammals, they are controlled by a complex bimodal regulation, which controls first the proximal patterning, then the distal structure, allowing at the same time the formation of the wrist and ankle articulations. We analyzed the implementation of this regulatory mechanism in chicken, i.e. in an animal where large morphological differences exist between fore- and hindlimbs. We report that while this bimodal regulation is globally conserved between mammals and avian, some important modifications evolved at least between these two model systems, in particular regarding the activity of specific enhancers, the width of the TAD boundary separating the two regulations and the comparison between the forelimb *versus* hindlimb regulatory controls. Some aspects of these regulations seem to be more conserved between chick and bats than with the mouse situation, which may relate to the extent to which forelimbs and hindlimbs of these various animals differ in their functions.

AUTHOR SUMMARY

The morphologies of limbs largely vary either amongst tetrapod species, or even between the fore- and hindlimbs of the same animal species. In order to try and evaluate whether variations in the complex regulation of *Hoxd* genes during limb development may contribute to these differences, we compared their transcriptional controls during both fore- and hindlimb buds development in either the mouse, or the chicken embryos. We combined transcriptome analyses with 3D genome conformation, histone

44 modification profiles and mouse genetics and found that the regulatory mechanism
45 underlying *Hoxd* gene expression was highly conserved in all contexts, though with some
46 clear differences. For instance, we observed a variation in the TAD boundary interval
47 between the mouse and the chick, as well as differences in the activity of a conserved
48 enhancer element (*CS93*) situated within the T-DOM regulatory landscape. In contrast to
49 the mouse, the chicken enhancer indeed displayed a stronger activity in fore- than in
50 hindlimb buds, coinciding with the observed striking differences in the mRNA levels.
51 Altogether, differences in both the timing and duration of TAD activities and in the width
52 of their boundary may parallel the important decrease in *Hoxd* gene transcription in chick
53 hindlimb *versus* forelimb buds. These differences may also account for the slightly
54 distinct regulatory strategies implemented by mammals and birds at this locus, potentially
55 leading to substantial morphological variations.
56

57 **INTRODUCTION**

58 Tetrapod limbs are organized into three parts bearing skeletal elements; the
59 stylopodium (humerus/femur), the zeugopodium (radius/fibula, ulna/tibia) and the
60 autopodium, the latter including the acropod (phalanges, metacarpals/metatarsals) and the
61 mesopodium (carpals and tarsals)[1]. Limbs can display large variations in their
62 morphologies, either between tetrapod species or within the same species, between fore-
63 and hindlimbs, as a result of their adaptation to different functions and ecological niches.
64 For example, frogs display particular shapes of carpal and tarsal elements, with an
65 elongated proximal tarsal whenever detectable[2], whereas geckos forelimb skeletal

66 elements somehow resemble those of their hindlimbs[3]. Another example of this
67 morphological flexibility are the forelimbs of bats, which do have digits early on similar
68 to those of other mammals but that subsequently elongate to make flight possible[4].

69 In this context, birds are a fascinating animal group as they evolved forelimbs
70 (wings) and hindlimbs (legs) specialized for flying or for terrestrial locomotion,
71 respectively[5]. Recent studies using comparative genomics approaches either amongst
72 birds or between bats and mice, have revealed that some DNA sequences potentially
73 involved in limb development and which are highly conserved can display differential
74 enhancer activities as compared to their mouse orthologous sequences[6,7]. Furthermore,
75 the analysis of several domestic pigeons displaying variations in foot feathering within
76 the same species, suggested that changes in cis-regulatory elements in the genes encoding
77 forelimb- or hindlimb-specific transcription factors may contribute to a partial
78 transformation from hindlimb to forelimb identity[8]. Taken together, these observations
79 suggest that both the gain of species-specific enhancers, the different activities of the
80 same regulatory sequences and alterations in DNA sequences amongst various species
81 and/or within the same species, contributed to generate these large morphological
82 differences.

83 In addition to their essential role during axial patterning and organogenesis in
84 vertebrates[9,10], *Hox* genes are required for proper growth and skeletal patterning of
85 tetrapod limbs. In particular, genes belonging to the *HoxA* and *HoxD* clusters for both
86 fore- and hindlimbs, as well as some genes of the *HoxC* cluster during hindlimb
87 development[11,12]. Regarding both *Hoxd* and *Hoxa* genes, recent development in

88 chromatin conformation techniques have made it possible to associate previously defined
89 limb regulatory landscapes to large chromatin interaction domains referred to as TADs
90 (topologically associating domains)[13–15]. Therefore, multiple limb-specific DNA
91 regulatory sequences were identified on either side of the *HoxA* and *HoxD* clusters,
92 grouped either into TADs and smaller sub-megabase large domains (sub-TADs)[16–19].
93 At the murine *HoxD* locus, two overlapping subsets of genes are controlled by the
94 two adjacent regulatory TADs located on the telomeric side (T-DOM) and the
95 centromeric side (C-DOM) of the cluster[17]. The region of the cluster extending from
96 *Hoxd1* to *Hoxd8* generates constitutive interactions with T-DOM, whereas the 5' region
97 of the cluster, which includes *Hoxd13* to *Hoxd12,* predominantly contacts C-DOM.
98 Interestingly, the genes from *Hoxd9* to *Hoxd11,* located within the boundary between
99 these two TADs, interact with both T-DOM and C-DOM, yielding their transcripts in
100 both the future zeugopod and acropod domain. In this situation, the expression of *Hoxd1*
101 to *Hoxd11* is driven by contacts with enhancer elements situated in T-DOM in the
102 prospective zeugopod. Then, as the future acropod domain is generated, *Hoxd* genes start
103 to weaken their interactions with T-DOM and *Hoxd9* to *Hoxd11* switch to establish
104 interactions within C-DOM. This switch is partly controlled by HOX13 proteins, which
105 inhibit T-DOM activity while re-enforcing C-DOM-located enhancers function[20]. This
106 bimodal regulatory mechanism allows the production of a domain of low *Hoxd*-
107 expression in which both T-DOM and C-DOM regulations are functionally inert, giving
108 rise to the future mesopodium. While this complex system seems to be globally conserved
109 throughout evolution[21,22], some slight modifications could readily lead to important

110 changes in expression specificities.

111 In different tetrapod species, the morphological diversifications seen in particular in
112 both the mesopod and the zeugopod between fore- and hindlimbs were suggested to result
113 from heterochronic variations in *Hox* gene expression[2][23]. Both gain of function and
114 loss of function experiments have revealed that either the ectopic expression or the mis-
115 regulation of *Hoxa13* and *Hoxd13* can induce a substantial reduction and malformation
116 of the zeugopod, similar to mesomelic dysplasia conditions in human families (e.g.[24]).
117 This is due to the potential of these particular HOX13 proteins to antagonize the function
118 of other HOX proteins to control and stimulate the ossification of limb skeletal
119 elements[25]. In this view, HOX protein production controlled by the T-DOM stimulate
120 bone growth, whereas C-DOM enhancers upregulate *Hoxd13* to antagonize this property,
121 leading to both smaller bones (phalanges) and the termination of the structure, in a dose-
122 dependent manner[26–30].

123 In this context, it was recently reported that a bat regulatory sequence located within
124 T-DOM and controlling *Hoxd* genes displays differential enhancer activity in the limbs,
125 when compared to its mouse orthologous sequence[6]. These findings suggest that some
126 variations in limb morphology may be associated with the mechanism of bimodal gene
127 regulation described at the *HoxD* locus. However, this mechanism was reported to be
128 implemented during the development of forelimb buds only and hence it remained unclear
129 as to how much the important differences between fore- and hindlimbs either amongst
130 various species or within the same species, may be related to variations of this mechanism.

131 To tackle this issue, we used a comparative regulatory approach involving chick and

132 mouse embryonic fore- and hindlimbs, mostly for two reasons. First chicken embryos,
133 unlike mice, display striking differences between the morphologies of their adult wings
134 (forelimbs) and legs (hindlimbs) (Fig. 1A, B, left). Secondly, it was reported that *Hoxd*
135 gene expression domains during chick wing- and leg buds development showed important
136 deviations when compared to their mouse counterparts[23,31]. These features suggested
137 that the bimodal regulatory system at work at the mouse *HoxD* locus may be operating
138 slightly differently during the development of the avian appendicular skeletons.

139 Here we combine analyses of transcriptome, 3D genome conformation, histone
140 modification and mouse genetics to show that this bimodal regulatory mechanism is
141 highly conserved in birds. However, in chicken leg buds, the duration of the T-DOM
142 regulation is much reduced, as suggested by dynamic changes in histone modifications,
143 along with a slight difference in chromatin interaction profiles at specific enhancer
144 regions, which accounts for the concurrent reduction in *Hoxd* genes expression in the
145 zeugopod. Finally, by using mutant mouse embryos lacking a large part of T-DOM, we
146 uncovered differences in the effect of T-DOM deletion for *Hoxd* genes between fore- and
147 hindlimbs. Therefore, while these regulatory mechanisms are virtually the same amongst
148 tetrapod species and even within the same species between the fore- and hindlimbs, slight
149 differences are scored, which may partly contribute to the observed morphological
150 differences.

151

152 **RESULTS**

153 **Transcription of *Hoxd* genes in mouse and chick limb buds**

154 We first compared the expression patterns of *Hoxd* genes in mouse fore- and
155 hindlimbs at E12.5 (Fig. 1A) with those observed in chick at either HH28 (equivalent to
156 E12.25 to E12.5) (Fig. 1B) or HH30 (equivalent to E13 to E13.5) (Fig. 1D). In mouse
157 fore- and hindlimbs, expression of *Hoxd13* and *Hoxd12* was strong in the prospective
158 acropod region (hereafter termed "distal"), whereas the domains of *Hoxd11* and *Hoxd10*
159 transcripts were split into the distal and zeugopod (hereafter termed "proximal") regions,
160 except the future mesopod, which was labelled by a *Col2a1*-expressing domain (Fig. 1A,
161 arrowheads). These expression patterns were similar in both fore- and hindlimbs, except
162 for a clearly weaker expression level in the hindlimb proximal domain.

163 When compared with *Hoxd* gene expression in the mouse counterparts, at least two
164 dramatic differences were confirmed in chick limbs. First, unlike the *Hoxd12* expression
165 pattern observed in murine limbs, the chick *Hoxd12* gene was strongly expressed in chick
166 proximal forelimb (wing) (Fig. 1B). Secondly, the expression of all *Hoxd* genes was
167 significantly reduced in the chick proximal hindlimb (leg) by stage HH28, when
168 compared to chick proximal wing and mouse proximal limbs[23,31]. As a result, the
169 expression domains of the chick *Hoxd12* in wing buds was much like that of *Hoxd11* or
170 *Hoxd10*, in contrast with the mouse where *Hoxd12* was never strongly expressed in the
171 proximal domain. However, the transition between the two *Hoxd*-expressing domains
172 also labelled the future wing mesopod (Fig.1B, arrowheads). Of note, expression of all
173 *Hoxd* genes was weak in proximal leg buds, again in contrast to what was observed during
174 mouse limb bud development (Fig. 1).

175 To characterize these differences in more detail, we performed RNA-seq analyses

176 by using HH30 limb buds in order to more easily micro-dissect the various domains and
177 thus exclude a potential contamination of the future mesopod from the distal domain.
178 RNA profiles confirmed the differences detected by WISH. First, *Hoxd11* to *Hoxd8* were
179 expressed at lower levels in the mouse proximal hindlimb when compared to forelimb, a
180 situation re-enforced in chick proximal leg where only a weak *Hoxd12* signal was
181 detected (Fig. 1C, D, upper tracks). In contrast, more reads were scored for *Hoxa10* to
182 *Hoxa11* in both mouse and chick proximal hindlimb when compared to forelimb (S1 Fig).
183 In the distal domains, transcription patterns and profiles from mouse and chick were
184 similar between fore- and hindlimbs, at both *HoxA* and *HoxD* clusters (Fig. 1C, D, lower
185 tracks, S1 Fig). However, the chick profile revealed a consistently higher transcription of
186 *Hoxd12*, which was as strong as *Hoxd13*, whereas the amount of transcripts in the mouse
187 counterpart was much lower than that for *Hoxd13* (Fig. 1C, D, lower tracks). Taken
188 together, these initial results indicated that both the expression status and the transcript
189 domains of *Hoxd* genes displayed significant differences, either amongst species or
190 within the developing fore- and hindlimb buds, in particular in chicken.
191
192 **Bimodal regulation in both fore- and hindlimb buds**
193 To determine to what extent these differences could result from variations in the
194 implementation of the bimodal regulatory mechanism, we performed comparative 4C-
195 seq analyses. We used a variety of viewpoints located at comparable positions to reveal
196 potential interactions in both mouse and chicken limb buds. To do this, we cross-
197 annotated *Hoxd* genes regulatory sequences identified in the mouse genome onto the

198 chick genome by using the LiftOver tool in UCSC. These annotations were then used for
199 all following experiments. In both fore- and hindlimbs, interactions were scored between
200 *Hoxd* genes and the regulatory sequences *island III* and *Prox*, as hallmarks of C-DOM
201 transcriptional activity, or with the *CS39* sequence as a proxy for T-DOM activity in
202 either the distal or the proximal region, respectively[17,18]. As seen in mouse forelimbs,
203 *Hoxd11* mainly contacted T-DOM sequences, especially *CS39*, in mouse proximal
204 hindlimb cells, i.e., in cells where T-DOM was fully active and where C-DOM was silent
205 (Fig. 2A, top). In contrast, in mouse distal hindlimb cells, it preferentially interacted with
206 C-DOM sequences such as *island III* and *Prox* (Fig. 2A, bottom). Quantification of
207 contacts indicated 75% of telomeric contacts in proximal forelimb cells and 50% in distal
208 forelimb cells, showing that *Hoxd11* had reallocated 25% of its global interactions toward
209 the C-DOM TAD in distal cells. Likewise, mouse hindlimb cells showed the same
210 interaction profiles, with 70% of telomeric contacts in proximal hindlimb cells and 45%
211 in distal hindlimb cells (Fig. 2A). This comparison indicated that the bimodal regulation
212 is virtually identical between fore- and hindlimbs in mouse.

213 We then examined the related interaction patterns in chick wing and leg cells by
214 using a region between *Hoxd11* and *Hoxd10* as a viewpoint (termed '*Hoxd10-11*'), i.e. a
215 sequence located as close as possible to the bait used in the mouse experiments. In chick
216 proximal wing cells, *Hoxd10-11* mostly interacted with the *CS39* and *CS93* regions
217 located in T-DOM, as well as with a region near the *Hnrnpa3* gene, where the distal TAD
218 border is observed in the murine locus (Fig. 2B, black arrowhead). These predominant
219 contacts with T-DOM were reduced in chick distal wing cells, as in the mouse, and 25%

220 of contacts were indeed reallocated to C-DOM sequences such as the chicken *island III*
221 and *Prox* counterparts. When compared to chick proximal wing cells, the global
222 interaction with the T-DOM was decreased from 81 to 70% in proximal leg cells. In
223 particular, the interactions between the *Hoxd10-11* bait and the *CS93* sequence in T-DOM
224 were lost in proximal leg cells, which may account for the significant reduction of *Hoxd*
225 expression in chick proximal leg buds (Fig. 2B, red arrows). In contrast, the interaction
226 established by the *Hoxd10-11* bait in chick wing and leg distal cells were comparable, as
227 expected from transcripts analyses, and interactions were observed up to around the
228 *Atp5g3* gene where the border of C-DOM TAD had been mapped in mouse (Fig. 2B,
229 white arrowheads).
230
231 **Different enhancer activity of mouse and chick CS93 in fore- *versus* hindlimbs**
232 The mouse *CS93* sequence contains the former *CS9* sequence[17], which was unable
233 to elicit any reporter gene expression in a mouse transgenic context (Fig. 3A). Likewise,
234 a larger murine sequence encompassing *CS9* and referred to as mouse BAR116 (Bat
235 Accelerated Region 116) did not show any enhancer activity in the limbs[6] (Fig. 3A). In
236 contrast, the bat BAR116 sequence was able to drive strong expression in transgenic
237 mouse forelimb buds whereas a weak activity was detected in hindlimb buds, correlating
238 with the different expression levels of *Hoxd10* and *Hoxd11* observed between bat fore-
239 and hindlimb buds[6] (Fig. 3A). This sequence was thus proposed as having evolved a
240 bat-specific function.
241 Therefore, low expression of *Hoxd* genes in proximal hindlimbs seems to be a

242 common feature of bats and chicken, suggesting that the chick *CS93* sequence may have
243 a limb enhancer activity similar to that reported for the bat BAR116. We examined the
244 enhancer activity of chick *CS93* using a transgenic mouse *lacZ* reporter system and
245 compared it to the activity of full-length mouse *CS93* sequence by using lentivector-
246 mediated transgenesis[32,33]. We initially cloned a 2kb large sequence containing chick
247 *CS93* and those surrounding sequences (Fig. 3B), which showed higher interactions with
248 *Hoxd10* to *Hoxd11* in the 4C profiles obtained from proximal wing cells (Fig. 2B, track
249 1). We noted that the surrounding sequences are not particularly conserved among species,
250 whereas the *CS93* region of the chick genome is more conserved with the bat than with
251 the mouse counterpart (Fig. 3B). By using the BLAT search tool in UCSC, we also found
252 that most of conserved regions from the bat BAR116 and the chick *CS93* sequences can
253 be aligned onto the mouse *CS9* region, respectively (Fig. 3A).

254 We assessed their enhancer activities and, unlike for the mouse BAR116, the full-
255 length mouse *CS93* triggered *lacZ* transcription in E10.5 limb buds with an expression
256 localized to the prospective stylopod and zeugopod at E12.5 (Fig. 3C). The staining was
257 weaker in hindlimb than in forelimb buds, possibly due to the delay in limb
258 development[34,35]. Accordingly, the 380bp localized in 5' of the mouse *CS93* seem to
259 be essential for expression. On the other hand, we found that the 2kb large sequence
260 containing the chick *CS93* displayed limb enhancer activity in mouse limb buds at E12.5
261 (Fig. 3D). The transgene expression driven by chick *CS93* came under two different
262 patterns. The first one displayed *lacZ* staining throughout the forelimbs (n=2/5), which
263 was similar to the staining observed when the bat BAR116 sequence was assessed in

264 mouse forelimb bud (Figs 3 and 4 in[6]). The second pattern concerned mostly the
265 proximal forelimb buds (n=3/5), as seen when the mouse *CS93* was used (Fig. 3C). In
266 both cases, a weaker expression was observed in hindlimb bud, as in the case of bat
267 BAR116. These results suggest that the downregulation of *Hoxd* genes in chick leg bud
268 involves a weaker activity of- and less interactions with the *CS93* sequence. Taken
269 together with previous research [6], these results indicate that, unlike for the bat BAR116
270 and the chick *CS93*, the mouse *CS9* is devoid of limb enhancer activity. Accordingly, the
271 380bp localized in 5' of the mouse *CS93* seem to be essential for expression.
272
273 **Implementation of the regulatory switch between TADs in mouse and chicken**
274 We observed that the differences in *Hoxd12* expression were more substantial
275 between chick fore- and hindlimb buds than in the murine counterparts (Fig. 1C, D).
276 Therefore, we wondered whether the regulatory switch from the T-DOM to the C-DOM
277 regulations would occur differently in the two species. We produced and examined 4C
278 interactions profiles by using *Hoxd12* itself as a bait. Similar to the profiles obtained with
279 the *Hoxd10-11* bait, we observed weaker interactions between *Hoxd12* and both the *CS39*
280 and *CS93* regions in T-DOM in chick proximal leg cells than in proximal wing cells (S2A
281 Fig, top). The profiles with the *Hoxd10-11* bait showed strong and stable interactions with
282 T-DOM, when compared with C-DOM, in both proximal and distal limbs (Fig. 2B). We
283 also found that *Hoxd12* mainly contacted T-DOM in both chick proximal wing and leg
284 cells, whereas it established more interactions with C-DOM in both chick distal cells
285 (S2A Fig, top and bottom).

286 The murine *Hoxd9* to *Hoxd11* genes, but not *Hoxd12*, are located within the TAD
287 boundary and interact both with T-DOM and with C-DOM. In contrast, in chicken limb
288 buds, *Hoxd12* was able to switch contacts from T-DOM to C-DOM, suggesting that the
289 TAD boundary in chick could be located between *Hoxd12* and *Hoxd13* (see also S2B and
290 S2C Fig) thus suggesting that the exact genomic interval where the switch in contacts
291 occurs between the genes and the TADs is displaced towards a more 5' position within
292 the chicken gene cluster, when compared to murine limb buds where this switch region
293 was localized around the *Hoxd11* locus[17,19]. This same switch was observed in both
294 chick wing- and leg bud cells, regardless of the various expression levels of *Hoxd* genes
295 in the proximal region, revealing that the switch between TADs is independent of *Hoxd*
296 expression itself in proximal cells.

297 These results showed that the bimodal regulatory mechanism and the sequential
298 transition from the proximal to the distal global controls are implemented during chick
299 limb development similarly to what was described in mice. Therefore, the differences in
300 gene expression observed both between mice and chicken and between chick wing- and
301 leg buds cannot be solely explained by visible variations in the respective interaction
302 profiles. Instead, they ought to involve the distinct use of enhancers (or group thereof-)
303 within an otherwise globally conserved chromatin architecture.

304

305 **Premature termination of the proximal TAD activity in chick leg buds**

306 Since the chromatin architecture at the *HoxD* locus is seemingly comparable
307 between mouse and chicken in both fore- and hindlimb buds, we looked for what may

308 cause the drastic reduction of *Hoxd* expression observed in chick proximal leg. Within
309 the T-DOM TAD structure, the interaction profiles obtained from chick leg proximal cells
310 showed reduced contacts between *Hoxd* promoters and enhancers in T-DOM (Fig. 2 and
311 S2 Fig). We complemented these observations by assessing the functional state of T-
312 DOM sequences by comparing particular histone modifications profiles between chick
313 wing- and leg buds, at several developmental stages (Fig. 4). We looked at the acetylation
314 of H3K27 (H3K27ac), a modification associated with transcriptional and enhancer
315 activity and at the trimethylation of the same residue (H3K27me3), a mark associated
316 with Polycomb-dependent silencing[36]. In both wing- and leg buds at stage HH19, a
317 stage which corresponds to ca. E9.5 in mouse, enrichments of H3K27ac were detected
318 over both T-DOM and the *HoxD* cluster itself, showing that the activation of *Hoxd* genes
319 by the T-DOM enhancers had been properly initiated in leg buds (Fig. 4A, tracks 1 and
320 2). Of note, higher levels of this mark were scored over the *Hoxd11* to *Hoxd13* region in
321 leg- than in wing buds (S3A Fig).

322 At stage HH20 (approximatively E10 in mouse), the H3K27ac enrichment in T-
323 DOM was still substantial in wing buds. In marked contrast, however, this level appeared
324 dramatically reduced in leg buds (Fig. 4A, tracks 3 and 4, region *a*), thus coinciding with
325 low gene expression (S3A Fig). The accumulation of H3K27ac observed near the TAD
326 border was specific for the early wing-bud (Fig. 4A, tracks 1 and 3, region *b*).
327 Furthermore, H3K27ac signals over C-DOM were not yet observed at these stages
328 (except around the island I region), in agreement with the fact that the regulatory switch
329 had not yet occurred. At a later stage (HH28, i.e. approximately E12.5 in mouse),

330 enrichment of H3K27ac within the *HoxD* cluster was significantly lost in proximal leg
331 bud cells where *Hoxd* expression was weak (Fig. 4A, track 6, S3A Fig). In contrast,
332 H3K27ac accumulation over the T-DOM in proximal wing bud cells remained, yet it
333 started to slowly decrease as observed in mouse proximal forelimb at E12.5 (Fig. 4A,
334 track 5). At the same time, H3K27ac was finally enriched over both C-DOM and the
335 *HoxD* cluster, in both wing- and leg distal cells, as scored in mouse distal forelimb buds
336 (Fig. 4A, tracks 7 and 8, S3A Fig)[17,20]. These various profiles showed that in chick
337 leg bud cells, the functional switch between T-DOM and C-DOM had occurred normally,
338 except that after its initial onset, T-DOM activity was terminated much more rapidly than
339 in the wing bud, followed by a decrease in accumulation of H3K27ac at the target *HoxD*
340 cluster itself.

341 We complemented these observations by analyzing H3K27me3 marks, which
342 antagonize the acetylation of the same residue[36]. At stage HH20, no H3K27me3 signal
343 was detected over T-DOM in both wing- and leg buds, except around *CS39* in leg buds
344 (Fig. 4B, tracks 1 and 2, region '*a'*), in agreement with the H3K27ac profiles (compared
345 with Fig. 4A, tracks 3 and 4). In contrast, strong levels of H3K27me3 enrichment were
346 observed over the C-DOM regions, where H3K27ac peaks were not detected (Fig. 4B,
347 tracks 1 and 2), suggesting that the activation of *Hoxd* genes by C-DOM regulation had
348 not yet occurred at this stage.

349 At the *HoxD* cluster itself, stronger levels of H3K27me3 enrichment were clearly
350 detected in leg buds, as compared with wing buds, from the pseudo-*Hoxd1* gene to *Hoxd8*,
351 a DNA interval controlled by T-DOM regulation (S3B Fig). At later stages, H3K27me3

352 marks were observed over C-DOM in proximal wing bud cells, where C-DOM is inactive,
353 whereas the levels of H3K27me3 marks over T-DOM, in both proximal and distal wing
354 bud cells, were comparable to those seen in the H3K27ac profiles (Fig. 4B, tracks 3, 5).
355 We had previously suggested that the binding of HOX13 proteins to sequences located in
356 T-DOM could cooperate with Polycomb complexes to terminate T-DOM regulatory
357 activity[20].

358 Altogether, the distribution of both H3K27ac and H3K27me3 marks in chicken limb
359 buds were in agreement with the observed expression status of *Hoxd* genes profiles. A
360 major difference was scored, however, when compared to their mouse counterparts. In
361 proximal leg bud cells at HH28 indeed, where *Hoxd* gene expression is quite weak (Fig.
362 4B, track 4; regions '*a*' and '*b*'), T-DOM and the *HoxD* cluster were heavily decorated
363 with H3K27me3 marks, in addition to the C-DOM TAD. The latter profile resembled that
364 obtained from distal leg bud cells at the same stage, i.e. cells where T-DOM is inactive
365 and completely shut down (Fig. 4B, track 6; regions '*a*' and '*b*'), suggesting that T-DOM
366 was not operational in proximal leg cells, unlike in the mouse forelimb proximal
367 situation[17,20].

368 We also examined the distribution of both H3K27ac and H3K27me3 marks over
369 the *HoxA* cluster and its limb regulatory landscape that maps within a sub-TAD adjacent
370 to *Hoxa13* [16](S4 Fig). H3K27ac distribution suggested an earlier activation of *Hoxa13*
371 in leg- than in wing buds at HH19 and HH20 (S4 Fig), which corroborated the
372 transcriptomes established at HH20 (S4C Fig). At HH28 however, the profiles of
373 H3K27ac and H3K27me3 marks over the *HoxA* cluster and within the flanking regions

374 were comparable between wing- and leg bud cells (S4 Fig) and did not show any of the
375 differences reported for the *HoxD* cluster and their regulatory landscapes. H3K27ac
376 profiles were similar over the *HoxA* limb enhancers in wing- and leg tissues at all stages,
377 except perhaps for a slight decrease in H3K27ac in leg bud at HH20 (S4A Fig).
378

379 **Chromatin conformations of the chicken *HoxD* cluster in wing- and leg buds**

380 Gene expression usually occurs concomitantly with enhancer-promoter
381 contacts[37–39]. Because of the dramatic difference in T-DOM activity observed in chick
382 leg- *versus* wing buds at stage HH20 (Fig. 4A, tracks 3 and 4, region '*a*'), we looked for
383 potential parallel differences in chromatin contacts by performing high-resolution capture
384 Hi-C analyses (CHi-C)[40,41] using wing- and leg buds at HH20. Since such a global
385 chromatin assessment had not been done during chick development, it also allowed us to
386 compare it with mouse counterpart cells and see to what extent these complex regulatory
387 systems were conserved in distinct groups of tetrapods.

388 The CHi-C profiles of chicken cells confirmed that the *HoxD* cluster is positioned at
389 the boundary between two TADs, similar to what was proposed in mouse limb bud
390 tissues[17,19] and the two sub-TADs seen in the murine T-DOM were detected as well
391 (S5A and S5B Fig). To position the boundary between the two TADs, we applied the
392 TopDom algorithm[42], which determined the border around the *Hoxd13* locus in both
393 wing- and leg bud cells at HH20 (Fig. 5A). This extended the conclusion reached after
394 the 4C analyses, i.e. that the TAD boundary region in chick was displaced towards the 5'
395 part of the gene cluster when compared to mouse limb bud cells[19].

396 In mouse limb cells, this TAD boundary falls within a region where multiple CTCF
397 sites are occupied[43–45]. CTCF is an architectural protein that both helps defining
398 constitutive domains of interaction and triggers enhancer-promoter contacts[46]. We thus
399 examined the presence of bound CTCF at the chick *HoxD* locus and surrounding TADs
400 and found that the profiles were comparable between wing- and leg buds at HH20 (S5
401 Fig). As for the mouse *HoxD* cluster[19], the orientations of the CTCF motives located
402 on either sides of the TAD boundary were facing those sites found in their flanking TADs,
403 suggesting the possibility for long-range loops to be established (S5C Fig, top)(e.g.[47]).
404 Noteworthy, the orientation of the CTCF motives were conserved between mouse and
405 chick. However, we found less bound CTCF in the chicken *HoxD* cluster than in the
406 mouse counterpart, which could affect the strength and/or stability of the TAD boundary
407 in chick (S5C Fig, bottom).

408 Using CHi-C at 5kb resolution, the distribution of contacts was relatively similar
409 between wing- and leg bud cell populations, despite the reduced level of H3K27ac in the
410 T-DOM and near the TAD border in leg bud cells described above. The contacts between
411 the *HoxD* cluster (galGal5, chr7:16,315,000-16,395,000) and the T-DOM region '*a*'
412 (galGal5, chr7: 16,045,000-16,255,000) were indeed comparable between wing- and leg
413 bud cells (Wilcoxon sum test, W=222,690, p-value=0.663) (Fig. 5B). However, when the
414 comparison was further limited to a 30kb large region including *CS93* (galGal5,
415 chr7:16,090,000-16,120,000) rather than to the entire region '*a*', the contact intensity in
416 leg bud cells was clearly below that scored in wing bud cells (W=5,495, p-value=0.0213).
417 These reduced contacts between *Hoxd* genes and the surroundings of region *CS93*

418 confirmed the observation made by looking at the 4C profiles obtained using the later
419 stage (HH30) (Fig. 2).

420 The fact that bound CTCF was not detected around the *CS93* region suggests that
421 CTCF-independent variations in enhancer-promoter interactions may participate to the
422 important decrease in *Hoxd* gene expression levels in leg bud cells. The decreased
423 contacts seen in leg bud cells were also scored between the *HoxD* cluster and around the
424 T-DOM border region *'b'* (galGal5, chr7: 15,910,000-15,985,000; W=32,746, p-
425 value=0.009415). The decrease in contacts between the *HoxD* cluster and both the *CS93*
426 and TAD border regions in leg bud cells was somehow compensated for by an increase
427 of interactions between the *HoxD* cluster and the 5' region of *CS39* where several bound
428 CTCF sites were observed. The 4C profiles obtained when using the *Hoxd10-11* bait
429 showed interactions with the 5' region of *CS39* in both chick proximal and distal cells,
430 suggesting that these stable contacts are associated with CTCF, as described in mouse
431 developing limb buds[48].

432

433 **Regulation of T-DOM by HOXA13**

434 We asked what may cause both the robust reduction in H3K27ac marks in chicken
435 T-DOM and the decrease in contacts between *Hoxd* genes and the *CS93* region in leg bud
436 cells at HH20. As it was reported that HOX13 proteins bind T-DOM-located sequences
437 concomitantly to its inactivation and that the absence of these proteins prevented T-DOM
438 to terminate operating[20,49], we re-assessed the expression dynamics of *Hoxa13*. We
439 found it expressed earlier in chick leg bud than in wing buds[31](S4C Fig), suggesting

440 that the exact timing of *Hoxa13* transcriptional activation may fix the duration of T-DOM
441 activity during limb development.

442 We examined this possibility by performing time-course *in situ* hybridization and
443 RT-qPCR experiments, using chick and mouse entire fore- and hindlimb buds from HH20
444 to HH22 and E10.5 to E10.75, respectively (Fig. 6). While these developmental stages
445 are not strictly equivalent between chick and mouse[50], they were selected because the
446 size difference between chick wing- and leg buds is not yet too large between HH20 and
447 HH22[51]. Also, *Hoxa13* starts to be expressed in mouse forelimb buds at around
448 E10.5[52]. While the onset of *Hoxa13* expression was detected in chick wing bud at
449 HH22, *Hoxa13* transcripts were already well present in chick leg bud at HH20-21 (Fig.
450 6A, left). Also, the expression level of this gene in leg buds was markedly stronger than
451 in wing buds (Fig. 6A, right). *Hoxa11* expression was also higher in chick leg buds than
452 in forelimb buds, as was also observed in the RNA-seq dataset (S4C and S6A Fig),
453 suggesting that the entire chicken *HoxA* cluster was activated in leg buds well before it
454 was switched on in wing buds. This was nevertheless not a general phenomenon for *Hox*
455 genes, for the expression of *Hoxd13* was comparable between wing- and leg buds (Fig.
456 6A, bottom and S6B, S6C Fig, left).

457 In the mouse, the development of the forelimb bud precedes that of hindlimb buds
458 by about half a day. In contrast, the initiation of both wing- and leg bud in chicken is
459 almost concomitant and the growth of the leg bud exceeds that of the wing bud[34,51].
460 However, even when considering these developmental differences, the dramatic
461 variations we scored between both the timing of *Hoxa13* activation and its transcript

462 levels between the chick wing- and leg buds were different from the situation observed
463 in murine fore- and hindlimb bud (Fig. 6B, top). Also, expression of other *Hoxd* genes
464 increased in both mouse fore- and hindlimb buds, as development proceeded (Fig. 6B
465 bottom, S6B and S6C Fig. right), unlike in chicken leg buds. Therefore, an inverse
466 correlation exists between the activation of *Hoxa13* on the one hand, and the
467 downregulation of *Hoxd* genes such as *Hoxd11* in chick leg bud on the other hand. This
468 correlation was observed neither in chick wing bud, nor in mouse limb buds, supporting
469 the idea that an early activation of *Hoxa13* induces a premature termination of T-DOM
470 activity in chick leg bud.

471 We looked whether the profiles of H3K27ac ChIP-seq and Hi-C data obtained from
472 chick limb tissues and covering the *HoxA* cluster would reveal traces of this early and
473 strong activation of *Hoxa13* seen in chick leg buds at HH20 (S4A and S6D Fig). While
474 this activation was consistent with enriched H3K27ac marks over the *HoxA* cluster itself,
475 it was not fully consistent with the distribution of chromatin marks over those enhancers
476 previously described to regulate *Hoxa13* in developing mouse limbs[16](S4A Fig). Hi-C
477 heat maps, however, showed increased contacts between the 5' region of the *HoxA* cluster
478 and its limb enhancer regions in leg bud at HH20, when compared to wing buds,
479 suggesting this may contribute to an early activation of *Hoxa* genes in leg buds (S6D Fig).
480

481 **Different impacts of T-DOM upon mouse fore- and hindlimb buds developments**

482 The importance of the T-DOM TAD for mouse proximal limb development was
483 initially assessed in forelimbs exclusively. The fact that birds displayed this striking

484 difference in T-DOM-dependent regulations in wing and leg buds suggested that tetrapod
485 fore- and hindlimbs may use the T-DOM enhancers in a slightly different manner. We
486 investigated this possibility by looking at the effect of a full deletion of T-DOM upon
487 *Hoxd* gene regulations in both murine fore- and hindlimb buds, in order to identify a
488 potential difference in the genetic requirements for T-DOM regulations between the two
489 contexts. We analyzed mouse limb buds carrying the *HoxD*$^{Del(attp\text{-}SB3)}$ allele, where an
490 approximatively 1Mb large region including the entire T-DOM as well as its distal border
491 was deleted. *Hoxd* transcripts produced in E12.5 proximal limbs by the *HoxD*$^{Del(attp\text{-}SB3)}$
492 allele (Fig. 7A left, *Del(attp-SB3)/*Δ) were scored by using both *in situ* hybridization and
493 RT-qPCR (Fig. 7A right, S7A Fig. left). In such mutant proximal forelimb buds, *Hoxd11*
494 to *Hoxd8* transcripts were depleted for more than 90% when compared to control
495 proximal forelimbs (Fig. 7A right, S7A Fig. left). Surprisingly however, *Hoxd11*
496 transcripts were not as dramatically affected in proximal mutant hindlimbs, and
497 transcripts produced by the *Hoxd10* to *Hoxd*8 genes were decreased in amount by 50 to
498 60% when compared to control animals (Fig. 7A right, S7A Fig. left). The reduced level
499 of *Hoxd* gene expression elicited by the mouse T-DOM deletion in the forelimb bud thus
500 mimics the situation observed in chick proximal leg bud (S7A Fig. right) and these
501 significant differences also exist in the way T-DOM operates in murine forelimb *versus*
502 hindlimb buds.

503 Interestingly, the sustained expression of *Hoxd* genes in T-DOM deletion mutant
504 proximal hindlimb buds completely disappeared when a larger deletion was engineered
505 between the *Mtx* and *Titin (Ttn)* genes (Fig. 7A), indicating that the genomic regions

506 between SB3 and *Ttn*, i.e. telomeric to the T-DOM TAD, contributes to the difference in
507 gene expression observed between the mouse fore- and hindlimb buds when T-DOM is
508 removed.

509 To identify potential forelimb to hindlimb differences in chromatin re-
510 organization after the deletion of T-DOM, we generated 4C profiles from the mutant
511 allele using the *Hoxd11* promoter as a viewpoint (Fig. 7B). In control proximal fore- and
512 hindlimb cells, *Hoxd11* mostly contacted the intact T-DOM, with a particularly strong
513 interaction with and around the CS39 region (Fig. 7B, tracks 1 and 3). In proximal cells
514 deleted for T-DOM, interactions within the *HoxD* cluster were increased and ectopic
515 contacts were established (or strongly re-enforced) with the newly fused neighboring
516 telomeric TAD (Fig. 7B, tracks 2 and 4). We used this 4C-seq dataset to determine three
517 candidate regions of potential enhancer activity, referred to as hindlimb enhancer (HE) 1
518 to 3 (Fig. 7B, C, red arrows). We cross-checked this selection either with DNaseI
519 hypersensitive sites (HS) data from E11.5 hindlimb buds (GSM1014179)[53], with
520 potential enhancer regions as defined by the Limb-Enhancer Genie tool[54] and with
521 H3K4me1 ChIP-seq datasets obtained from control and mutant hindlimb proximal
522 domains (Fig. 7C and S7B Fig). According to these criteria, HE1 turned out to be the
523 most promising region and we thus assessed its enhancer potential in developing
524 transgenic limb buds.

525 By using a transgenic enhancer reporter system, the HE1 region reproducibly drove
526 *lacZ* expression in proximal fore- and hindlimb buds, lateral plate and somatic mesoderm
527 at E12.5 (Fig. 7D). This result indicated that the HE1 enhancer activity is not specific for

528 the proximal hindlimb, even though it was potentially active in a hindlimb-specific
529 manner after deletion of T-DOM. To confirm this observation, we performed a 4C-seq
530 analysis by using the HE1 sequence as a bait (S7C and S7D Fig), using both control and
531 T-DOM deleted mutant proximal hindlimb cells. The 4C-profiles revealed that the HE1
532 sequence established slightly more contacts with the *Hoxd9* to *Hoxd12* DNA interval in
533 mutant than in control hindlimb cells.

534 Finally, we looked at potential genetic interactions between the limb-specific
535 differences in *Hoxd* gene expression and the *HoxC* gene cluster. Both *Hoxc10* and *Hoxc11*
536 are indeed strongly transcribed in proximal cells of hindlimb buds (*Hoxc11* in S7E Fig),
537 whereas these transcripts were not detected in the equivalent forelimbs territories[55].
538 Furthermore, in proximal hindlimbs where *Hoxc* genes are expressed, the amount of *Hoxd*
539 transcripts is decreased when compared to forelimb buds (Fig. 1C). Also, the deletion of
540 *Hoxc11* on top of *Hoxa11/Hoxd11* double knockout mice exacerbated the observed
541 hindlimb malformations[11][56], suggesting that HOXC proteins in hindlimb buds may
542 help maintaining *Hoxd* transcripts, a function that would become visible in the absence
543 of T-DOM, when *Hoxd* genes are no longer transcribed in forelimb proximal cells. We
544 thus performed *in situ* hybridization for *Hoxd11* by deleting the entire *HoxC* cluster[57]
545 on the top of the deletion of T-DOM. In these combined mutant limb buds, expression of
546 *Hoxd11* was still detected in hindlimb proximal cells, indicating that the persistence of
547 *Hoxd11* expression in hindlimb buds in the absence of T-DOM did not depend upon the
548 presence of hindlimb proximal cells-specific *Hoxc* transcripts.
549

550 **DISCUSSION**

551 **Conservation of the bimodal regulation in birds**

552 While the expression of *Hox* genes belonging to the *HoxA*, *HoxC* and *HoxD* clusters
553 during limb development are globally comparable between mammals and birds, some
554 clear differences are nevertheless apparent, such as the quasi absence of *Hoxd* genes
555 transcription in the proximal part of the developing leg buds in birds, while their
556 expression there is required for proper mouse hindlimb development[56,58]. Also, while
557 *Hoxd12* is expressed in the mouse limb buds like *Hoxd13*, i.e. mostly under the control
558 of C-DOM only, its expression in the avian wing buds resembles that of *Hoxd11*, i.e.
559 involving also the control of T-DOM, in future zeugopod cells. Because these expression
560 specificities depend on the implementation of global regulations located within the two
561 TADs flanking the *HoxD* cluster, we wondered whether the structures of these TADs
562 were somehow modified in birds, or at least whether they would show some variations
563 either between the two species, or between the bird wing and leg buds.

564 A global analysis of 4C and capture Hi-C datasets did not reveal any salient
565 differences between mammals and birds regarding the way they implement this complex
566 bimodal limb regulation at the *HoxD* locus. The TADs appeared well conserved between
567 the two species, as well as the presence in chick of most -if not all- regulatory elements
568 that had been described in the mouse counterparts, on both sides on the gene
569 cluster[17,18], even though the chick TADs were reduced in size. We thus conclude that
570 the bimodal regulatory strategy described in mammals (see[59]) is implemented in a
571 similar manner during bird development. This re-enforces the idea that the function of

572 *Hox* genes at these early steps of limb development is mostly to set up and organize the
573 basic plan of the future appendages, rather than elaborating or fine-tuning on a pre-
574 patterned structure.
575
576 **Interspecies comparison of the TAD boundary at *HoxD***
577 The bimodal regulatory mechanism and the transition between the two global
578 controls at *HoxD* are thus well conserved amongst tetrapods. However, the distinct
579 expression of *Hoxd12* in proximal limbs between mouse and chick suggests that the width
580 of the TAD boundary at the *HoxD* locus may slightly vary between the two species. By
581 using transcriptome, 4C and Hi-C datasets, we previously observed slightly different
582 positions of this boundary in mouse distal *versus* proximal limb cells, due to the fact that
583 *Hoxd10* and *Hoxd11* respond to both T-DOM and C-DOM regulations. We thus proposed
584 that the boundary was located between *Hoxd11* and *Hoxd12* in proximal cells, while
585 between *Hoxd9* and *Hoxd10* in distal cells[17,19] (Fig. 8A).
586 In contrast, the chick *Hoxd12* is strongly expressed in proximal wing buds,
587 suggesting that the TAD boundary, in this context, expands towards the 5' part of the
588 gene cluster, close to the *Hoxd13* locus (Fig. 8B). Our CHi-C analysis re-enforced this
589 view and positioned this boundary around the *Hoxd13* gene in chick limb buds at early
590 stages (HH20), i.e. when T-DOM is active and controls the first phase of *Hoxd* genes
591 transcription (S5 Fig). Subsequently (HH30), the boundary region was slightly reduced
592 from *Hoxd13* to an area between *Hoxd13* and *Hoxd12* in chick limbs. Of note, *Hoxd12* is
593 expressed in proximal limbs in geckos as in chicken[23], suggesting that the TAD

594 boundary at the *HoxD* locus in proximal buds may have been slightly shifted during
595 tetrapod evolution between birds and squamates on the one hand, and mammals on the
596 other hand.

597 Different tetrapod species may thus display various positions of their TAD
598 boundaries at *Hox* loci, acting as morphological cursors that would redistribute the
599 various sub-sets of *Hox* genes responding to either proximal or distal enhancers. The
600 distinct topologies of these boundaries may rely upon differences in the distribution
601 and/or usage of CTCF binding sites. In the mouse, subsets of genes responding to either
602 proximal or distal limb enhancers are delimited by different sets of bound CTCF sites
603 [19] (Fig. 8A). Here, we show that chicken wing bud cells have less bound CTCF sites
604 and of reduced intensity in the *HoxD* cluster than their murine counterparts, which could
605 modulate the positioning of the boundary. In this case, the decrease in the overall strength
606 of the boundary effect as a result of having less sites occupied by CTCF, may explain the
607 extension of interactions up to *Hoxd12-Hoxd13* established by proximal enhancers (Fig.
608 8B). This hypothesis could nevertheless not be verified on chicken leg proximal cells as
609 these cells do not strongly express the genes controlled by T-DOM.

610

611 **Distinct T-DOM regulations in mouse, chick and bat fore- and hindlimb buds**

612 During bat limb development, *Hoxd10* and *Hoxd11* transcripts are progressively lost
613 throughout the hindlimbs only, in part due to the distinct enhancer activity of the BAR116
614 sequence located within T-DOM[6]. When the mouse BAR116 cognate sequence was
615 used in a transgenic context, no activity was detected in any limb cells. Likewise, when

616 we used mouse *CS9*, i.e. a shorter fragment of the *CS93* sequence, staining was not
617 observed. However, when the full length *CS93* sequence was injected, a robust enhancer
618 activity was scored in a proximal limb region (Fig. 3). This discrepancy between two
619 experiments involving almost the same sequences may be caused by the positions of the
620 regions used for the mouse transgenic enhancer assays, the mouse sequence extending a
621 bit more towards one of its extremities. Either the enhancer activity was provided by this
622 sub-fragment, or this fragment may be required for the expression of a more widespread
623 activity of the full DNA sequence. It remains that the BAR116 sequence may not be a bat
624 specific enhancer.

625 However, while the bat BAR116 showed different enhancer activities between the
626 mouse transgenic fore- and hindlimb buds, i.e. strong in forelimb and weak in hindlimb,
627 the mouse equivalent appeared to have similar enhancer activities between fore- and
628 hindlimbs, in agreement with the continuous expressions of *Hoxd10* and *Hoxd11* in both
629 types of limbs. To further validate this correspondence, we looked at the behavior of the
630 chick *CS93* sequence in the same mouse transgenic context. While two sets of patterns
631 were obtained with various distal to proximal distributions of the *lacZ* staining, a clear
632 imbalance was scored between forelimb and hindlimb cells, with a much stronger
633 expression in the former than in the latter. Therefore, the chick enhancer sequence
634 behaved more like the bat sequence than like their murine counterparts, an effect that was
635 re-enforced by the sequence alignments, which revealed more similarities between chick
636 and bats than between the two mammalian species. This similarity correlates with *Hoxd*
637 gene expression and may relate to the salient distinctions in morphologies between fore-

638 and hindlimbs.

639

640 **Premature termination of T-DOM regulation in chick hindlimb buds**

641 The termination of the T-DOM regulatory activity in proximal limb cells coincides
642 with the binding of the HOXA13 protein at various sites within the TAD. Also, the
643 removal of both *Hoxa13* and *Hoxd13* functions lead to the continuation of T-DOM
644 regulation and to the failure of C-DOM activation, suggesting that HOX13 proteins are
645 necessary to terminate T-DOM function and to implement the bimodal switch[20,49].
646 The chick *Hoxd13* gene starts to be expressed at around stage HH18-19[31] when
647 H3K27ac enrichment is not yet detected over C-DOM (except for *island I*)(Fig. 4).
648 Instead, H3K27me3 marks are still present over C-DOM at this early stage, unlike in the
649 early mouse limb buds (Fig. 4 and S3 Fig)[17], suggesting that *Hoxd13* early activation
650 in chick may be driven by the T-DOM regulation until the C-DOM regulation is
651 implemented and takes it over. This idea is well supported by our CHi-C analysis showing
652 that the TAD boundary is expanded towards the *Hoxd13* locus in the early chick limb
653 buds.

654 In addition, a major difference was observed in the activation of *Hoxa13* between
655 chick and mouse hindlimb buds, with an earlier and stronger activation of *Hoxa13* in
656 chick leg buds at HH20, when compared to both mouse hindlimb buds and chick wing
657 buds. This indicates that the T-DOM activity may be readily terminated by the early
658 presence of HOXA13 protein and that the C-DOM regulation is ready to be active earlier
659 in chick leg buds than in wing buds. The potential causes for both this early activation of

660 *Hoxa13* in chick leg buds and the strong level of H3K27me3 observed over C-DOM in
661 chick wing and leg buds remain to be determined.
662
663 **Enhancer reallocation and anterior-posterior (AP) position of the limb buds**
664 In the mouse, we show that the deletion of the telomeric TAD has different effects
665 upon forelimb and hindlimb proximal cells, as fair levels of *Hoxd* gene expression remain
666 only in the proximal hindlimb domain. Since a larger deletion including more telomeric
667 sequences totally abrogated *Hoxd* expression in proximal hindlimb, we concluded that
668 additional hindlimb-specific enhancers may be located telomeric of the T-DOM TAD.
669 Interaction profiles established after the deletion of T-DOM revealed novel hindlimb-
670 specific contacts between target *Hoxd* genes and the newly identified HE1 sequence,
671 which is normally located outside T-DOM but brought to the vicinity of the cluster after
672 the deletion. The HE1 region is located near the *Agps* and *Pde11a* genes and our 4C
673 profile using HE1 as a bait showed strong interactions with both genes under normal
674 condition. Noteworthy, *Agps* is involved in the rhizomelic chondrodysplasia punctate 3
675 (RCDP3) condition, with a shortening of proximal limbs[60,61], suggesting that HE1
676 may be involved in the regulation of the *Agps* gene. The deletion of T-DOM may thus
677 reallocate part of the HE1 proximal limb enhancer activity towards *Hoxd* promoters.
678 Our genetic approach however makes it difficult to assess whether this sequence is
679 used for *Hoxd* regulation under normal circumstances, or whether the interactions
680 observed are mostly due to its new proximity to the target genes induced by the deletion
681 of T-DOM. In the former case, this may indicate that as in chick and bats, the global C-

682 DOM regulation may be more active in forelimb than in hindlimb buds and hence the
683 HE1 enhancer may not be necessary. In the case of the mouse, this deficit of regulation
684 during proximal hindlimb development could have been compensated for by evolving
685 additional enhancers outside the TAD (Fig. 8C). The HE1 sequence is bound by several
686 factors, such as the YY1, proposed to mediate enhancer-promoter contacts at distance in
687 ESCs[62], or PITX1, a hindlimb-specific factor[63], suggesting that multiple
688 transcriptional factors may contribute to this interaction.

689 Finally, the sustained expression of *Hoxd* genes observed in T-DOM deleted mutant
690 proximal hindlimb cells may merely reflect the history of early limb bud cells. In the wild
691 type condition indeed, the anterior bud emerges from a field of lateral plate mesoderm
692 (LPM) devoid of transcripts for *Hoxd9*, *Hoxd10* or *Hoxd11*. In contrast, posterior limb
693 buds derive from LPM cells already expressing these genes, due to their more posterior
694 AP position along the trunk mesoderm. In the absence of T-DOM, expression of these
695 genes would not occur in the anterior buds due to their repressed state and the lack of
696 appropriate enhancers, whereas expression could be inherited and maintained in the
697 posterior buds through a mechanism independent of T-DOM, perhaps involving the HE1
698 sequence.

699

700 **Materials and Methods**

701 **Animal experimentation**

702 All experiments involving animals were performed in agreement with the Swiss law on
703 animal protection (LPA), under license No GE 81/14 (to DD). Chick embryos from a

704 white Leghorn strain were incubated at 37.5°C and staged according to ref[51].

705

706 ***In situ* hybridization and *lacZ* staining**

707 Whole mount *in situ* hybridization was performed as described previously[64]. For *lacZ*
708 staining, embryos were fixed in 1x PBS pH7.39-7.41, 2mM $MgCl_2$, 4% PFA/PBS, 0.2%
709 glutaraldehyde and 5mM EDTA for 20 min at room temperature and washed three times
710 for 20 min in 1x PBS, 2mM $MgCl_2$, 0.2% NP40 and 0.01% sodium deoxycholate.
711 Samples were stained in 5mM potassium ferrocyanide, 5mM potassium ferricyanide and
712 0.5 mg/ml X-gal at room temperature overnight, followed by wash with the wash solution
713 once and refixation with 4%PFA/PBS at 4°C overnight.

714

715 **Micro-dissection chick limbs at HH30**

716 Limb tissues at HH30 were micro-dissected into acropod (distal), mesopod and zeugopod
717 (proximal) regions, respectively. Only distal and proximal regions were used for RNA-
718 seq and 4C-seq.

719

720 **RNA-seq and Data analysis**

721 Total RNA was extracted from mouse and chick limb bud tissues using the RNeasy Micro
722 Kit (QIAGEN) following the manufacturer instructions. Libraries were prepared with at
723 least 200 ng of total RNA following Illumina TruSeq stranded mRNA sample preparation
724 guide. Sequencings were performed with 100-bp or 75-bp single-end. The data was
725 mapped onto either GRCm38 (mm10) or the International Chicken Genome Reference

726 Consortium Gallus_gallus-5.0 (galGal5) using the Tophat2 (Version 2.0.9)[65] and
727 unique mapped reads were extracted. The number of uniquely mapped reads was
728 calculated using FLAGSTAT (SAMtools, Version 0.1.18)[66] and this value was used
729 for the subsequent normalization of each coverage data to be the million reads number.
730 All analyses were processed by our Galaxy server (the Bioteam Appliance Galaxy Edition,
731 https://bioteam.net, https://bioteam.net/products/galaxy-appliance)[67].
732
733 **RNA extraction and RT-qPCR**
734 Total RNA was extracted using the RNeasy Micro Kit (QIAGEN), following the
735 manufacturer instructions. 1 μg total RNA was used for cDNA synthesis with SuperScript
736 VILO (Invitrogen). RT-qPCR was performed on a CFX96 real-time system (BIORAD)
737 using the GoTaq qPCR Master Mix (Promega). Each RT-qPCR was carried out with at
738 least two biological replicates and each experimental information is described in S1 Table.
739 Primer sequences for qPCR are listed in S2 Table.
740
741 **4C-seq and Data analysis**
742 Each mouse and chick limb tissue were fixed separately with 2% formaldehyde, lysed
743 and stored at -80°C. Samples were digested with *NlaIII* and *DpnII* as primary and
744 secondary restriction enzymes, respectively, and ligation steps were performed using high
745 concentrated T4 DNA ligase (Promega)[68]. Inverse PCRs for amplification were carried
746 out using primers for each viewpoint[69](S3 Table). PCR products were multiplexed and
747 sequenced with 100bp single-end, followed by post-processing (de-multiplexing,

748 mapping, and 4C analysis) using the HTS station (http://htsstation.epfl.ch)[70]. Fragment
749 scores were normalized to the mean score of fragments falling into a region defined as
750 the bait coordinated ± 1 Mb, and the data were smoothed by using a running mean with
751 a window size of 11 fragments. The information regarding fragments excluded during the
752 procedure is provided in S3 Table. A relative quantification of the signal spanning both
753 the *HoxD* telomeric or centromeric domains was performed. Genomic coordinates for
754 calculations are:
755 mm10, chr2: 73,921,943-74,648,943 / chr2: 74,765,943-75,601,943;
756 galGal5, chr7: 15,920,642-16,318,067 / chr7: 16,414,183-16,699,172.
757 This quantification is not absolute and only reflects the balance of contacts between the
758 two domains, for each sample.
759
760 **ChIP-seq and Data analysis**
761 Chromatin immunoprecipitation experiments were performed as previously
762 described[20]. Micro-dissected limb tissues from mouse and chick embryos were cross-
763 linked with 1% formaldehyde/PBS for 15 min at room temperature. Chromatin was
764 sheared and used for each immunoprecipitation with anti-H3K27ac (ab4729, Abcam),
765 anti-H3K27me3 (07-449, Merck Millipore), anti-H3K4me1 (ab8895, Abcam) and anti-
766 CTCF (61311, Active Motif). Libraries were prepared with at least 5 ng of purified DNA
767 following Illumina TruSeq ChIP library preparation guide. Sequencing was performed
768 with 100bp single-end. Demultiplexed ChIP-seq reads were mapped onto the galGal5 or
769 mm10 using Bowtie (Version 0.12.7)[71], with parameters "-m1 –strata –best" according

770 to conditions described previously[72], and PCR duplicates were removed from mapped
771 reads using SAMtools (Version 0.1.18)[66]. By using bamCompare (Version 2.5.0), the
772 ChIP data from H3K27ac, H3K27me3 and H3K4me1 and the input data were normalized
773 and compared to compute the log2 of the number of reads ratio. The CTCF ChIP data
774 was normalized to obtain 1x depth of coverage by using bamCoverage (Version
775 2.5.0)[73,74]. The CTCF motif orientation analysis was performed as previously
776 described[19]. All analysis was done with our Galaxy server (the Bioteam Appliance
777 Galaxy Edition, https://bioteam.net, https://bioteam.net/products/galaxy-appliance)[67].
778

779 **SureSelect probe design and Capture Hi-C (CHi-C)**

780 The library of SureSelect enrichment probes were designed over the genomic interval
781 (galGal3: chr7:15,990,001-19,170,000) using the SureDesign online tool of Agilent.
782 Probes cover the entire genomic region (galGal5, chr.7: 14,946,000-17,870,000) and
783 were not designed specifically in proximity of *DpnII* sites. Dissected tissues were
784 dissociated in 10% FCS/PBS with collagenase (C7657, Sigma) to a final concentration
785 of about 1.3 μg/μL, and samples were incubated in Thermomixer at 37°C at 800 rpm for
786 20 min. After discarding the supernatant, cells were crosslinked with 1%
787 formaldehyde/PBS at RT for 10 min, quenched with glycine and centrifuged to discard
788 the supernatant. Cells were resuspended with PBS containing proteinase inhibitor and
789 then centrifuged again. After removing supernatant, cells were kept at -80°C before use.
790 Hi-C library preparation was performed as described in[75], with the following changes:
791 (i) Resuspended crosslinked cells in ice-cold Lysis buffer were placed on a rotation wheel

792 at 4°C at 30 rpm for 30 min for cell lysis. (ii) For chromatin digestion, 400U of *DpnII*
793 (R0543M, New England Biolabs) were added to the samples and incubated at 37°C at
794 700 rpm for 4 hrs. Another 400U of *DpnII* were added and samples were incubated
795 overnight. (iii) Blunt-end ligation of biotin filled-in DNA was performed at RT at 30 rpm
796 on rotating wheel for 4 hrs. (iv) No removal of biotin from un-ligated ends was performed.
797 (v) DNA was sheared to a size of 200 to 800bp by using COVARIS E220, with the
798 following conditions; 175W, 10% Duty factor, 200 Cycles per Burst, 60 sec. (vi) DNA
799 pulldown was performed by using Dynabeads MyOne Streptavidin T1 (65601, Thermo
800 Fisher). (vii) DNA was measured by Qubit and 200ng were used for further treatment
801 followed by manufacturer's protocol (SureSelect^{XT} Target Enrichment System for
802 Illumina Paired-End Multiplexed Sequencing Library).
803
804 **CHi-C data analysis**
805 Paired-end sequencing data were processed as follows. First, adapters were removed
806 using cutadapt version 1.6[76] with the following parameters: -a
807 AGATCGGAAGAGCACACGTCTGAACTCCAGTCAC for R1 and -a
808 AGATCGGAAGAGCGTCGTGTAGGGAAAGAGTGTAGATCTCGGTGGTCGCCG
809 TATCATT for R2. They were then processed by using hicup version 6.1.0 with the
810 bowtie2 version 2.2.6[77] and SAMtools version 1.2[66], with galGal5 as reference
811 genome and GATC as restriction enzyme recognition sequence. The pairs were next
812 converted from bam to tabulated files, with the position of the middle of the fragment to
813 which hicup assigned the read, by using an ad-hoc python script (available upon request).

814 Only valid pairs with both MAPQ above 30 were kept. Then, pairs with both mates in the
815 capture region (galGal5, chr7:14,946,000-17,870,000) were extracted and processed with
816 cooler to obtain a balance matrix of the capture region with 5kb bins. The Fig. 5 and S5
817 Fig were obtained with personal R scripts (available upon request) (http://www.R-
818 project.org). S5A and S5B Fig are the balanced matrices with linear scale. Fig 5 was
819 obtained by subtracting the two balanced matrices. To assess the significance of increased
820 contact between two regions, a Wilcoxon rank sum test was performed using R with the
821 values of the bins in the region of the two balanced matrices. Because 75% of valid pairs
822 MAPQ30 do not involve the capture region, all valid pairs were also processed with
823 cooler to obtain a balance matrix of the whole chromosome 2 at 40kb. These matrices
824 were used in S6 Fig. To define TAD borders (Fig 5), the TopDom algorithm[42] was run
825 with a window size of 28 from the 10kb binned balanced matrices, as gaps were too
826 numerous at a 5kb resolution.
827
828 **Mutant stocks**
829 The *HoxD*$^{Del(8\text{-}13)}$ and *HoxD*$^{Del(attp\text{-}SB3)}$ alleles have been previously described[17,78]. The
830 *HoxD*$^{Del(Mtx\text{-}Ttn)}$ allele was produced by TAMERE using the TiE2 (*Titin* exon 2) allele[79]
831 (kindly provided by Dr. Michael Gotthardt) and a *Mtx2* gene trap allele
832 (https://igtc.org/cgi-bin/annotation.py?cellline=CSI574). The sequences of genotyping
833 primers are indicated in S2 Table. All embryos analyzed in Fig 7 and S7 Fig were
834 heterozygotes, balanced by the *HoxD*$^{Del(8\text{-}13)}$ allele.
835

836 **Analysis of sequence alignment and limb enhancer prediction**

837 mVista, tools for comparative genomics was used for comparison between sequences of
838 the mouse *CS93* (mm10, chr2: 75,208,103-75,210,328), the bat BAR116 (Myoluc2,
839 GL429772: 6,606,808-6,608,652) and the 2kb region containing the chick *CS93* (galGal5,
840 chr7: 16,104,863-16,106,863), with LAGAN alignment program with default parameter
841 (http://genome.lbl.gov/vista/index.shtml). Potential limb enhancer regions were
842 identified by using Limb-Enhancer Genie tool, with the following condition: (i) analysis
843 type: Scan for top, (ii) method: Combined Model (https://leg.lbl.gov/)[54].

844

845 **Enhancer transgenic assays**

846 For the enhancer assays, embryos carrying the mouse *CS93/lacZ* and *HE1/lacZ* were
847 generated by lentivirus-mediated transgenesis and pronuclear injection, respectively. The
848 mouse *CS93* (mm10, chr2: 75,208,104-75,210,328) was amplified from C57BL/6
849 genomic DNA and cloned into the *pRRL-lacZ* vector, as described previously[17].
850 Lentiviruses were produced and injected into the peri-vitelline space of mouse
851 zygotes[32]. The mouse *HE1* (mm10, chr2: 75,959,179-75,960,378) and the region
852 containing the chick *CS93* sequence (galGal5, chr7: 16,104,863-16,106,863) were
853 obtained from B6CBAF1/J and White Leghorn genomic DNA, respectively, and cloned
854 into a *βglobin-lacZ* vector. The construct was injected into mouse oocytes. All transgenic
855 embryos were harvested between E10.5 and E12.5 and used for *lacZ* staining.

856

857 **Accession Numbers**

858 RNA-seq, 4C-seq, ChIP-seq and CHi-C datasets are available from the NCBI Gene
859 Expression Omnibus repository under accession number GSE115563. The public datasets
860 used in this research are listed in S4 Table.
861
862 **ACKNOWLEDGEMENTS**
863 We thank Dr. A. Necsulea for help with bioinformatic analyses, S. Gitto and T.-H.
864 Nguyen Huynh for technical help, Drs. J.-M. Matter, M. Gotthardt, M. Ros, C. Tabin, Y.
865 Kawakami and K. Tamura for sharing materials, the Geneva Genomics Platform
866 (University of Geneva), the transgenic core facilities (University of Geneva and Ecole
867 Polytechnique Fédérale in Lausanne), the Gene Expression Core Facility, the
868 Bioinformatics and Biostatistics Core Facility of the Ecole Polytechnique Fédérale in
869 Lausanne and the ENCODE Consortium and the ENCODE production laboratory
870 generating the particular dataset. We also thank all members of the Duboule laboratories
871 for discussions.
872
873 **Author Contributions**
874 Conceptualization: N.Y.-K., G.A. and D.D.
875 Methodology: N.Y.-K., G.A., C.C.B. and D.D.
876 Investigation: N.Y.-K., C.C.B., G.A. and L.B.
877 Formal Analysis: N.Y.-K. and L.L.-D.
878 Writing-Original Draft: N.Y.-K., L.L.-D. and D.D.
879 Writing-Review and Editing: L.L.-D., G.A., L.B. and C.C.B.

880 Supervision and funding: D.D.

881 **LEGENDS TO FIGURES**

882 **Fig. 1. *Hoxd* genes expression in mouse and chick limb buds.** (A, B) *In situ*
883 hybridization analysis of E12.5 mouse and HH28 (equivalent to E12.25 to E12.5) chick
884 fore- and hindlimb buds showing the expression of *Hoxd* genes and *Col2a1* or *Aggrecan*,
885 which are markers for chondrocyte differentiation. (A, left) Schemes showing
886 morphologies of forelimb (red) and hindlimb (yellow) in mouse. (A, right) Expression
887 patterns of *Hoxd* genes in forelimb buds are comparable to those in hindlimb buds. The
888 expression domain of *Col2a1* (opened arrowheads) corresponds to the low *Hoxd*
889 expression region leading to the future mesopodium. (B, left) Schemes representing
890 morphologies of forelimb (wing, red) and hindlimb (leg, yellow) buds in chick. (B, right)
891 Expression of *Hoxd* genes in proximal leg is significantly reduced and restricted to the
892 presumptive ulna. (C, D) Transcription profiles of *Hoxd* genes in micro-dissected
893 proximal and distal domains, either from E12.5 mouse (C) or HH30 (equivalent to E13
894 to E13.5) chick (D) fore- and hindlimb buds. Each right limb in (A, B) is oriented with
895 proximal to the bottom and distal to the top. FL, forelimb; HL, hindlimb. The *Y* axis
896 represents the strand-specific RNA-seq read counts, normalized by the total number of
897 million mapped reads.

898

899 **Fig. 2. Conserved bimodal TAD regulatory structure at *HoxD* locus in tetrapod.**
900 (A, B) 4C-seq tracks showing contacts established by mouse *Hoxd11* and chick *Hoxd10-*
901 *11* viewpoint in mouse and chick proximal and distal cells from fore- and hindlimb at
902 E12.5 and HH30, respectively. (A) The interactions between *Hoxd11* and around *CS39*

903 were mainly observed in proximal cells, whereas those between *Hoxd11* and *island III* or
904 *Prox*, which are hallmarks of the C-DOM activity, were increased in distal region. (B)
905 Each contact extended to the predicted TAD border located on either side at *HoxD* cluster
906 (C-DOM side, opened arrowheads; T-DOM side, closed arrowheads). In addition to the
907 interactions between *Hoxd10-11* and *CS39*, contacts were also observed with *CS93* in
908 proximal wing bud cells, whereas it decreased in proximal leg bud cells where *Hoxd*
909 expression is strongly reduced (red arrows). FL, forelimb; HL, hindlimb.
910
911 **Fig. 3. Differential enhancer activities of mouse and chick *CS93* in fore- and**
912 **hindlimb buds.** (A) Genomic coordinates and sequence alignment using either the bat or
913 the chick sequence onto the mouse genome, and schematics of enhancer activities for
914 each of the identified sequences[6,17] and this work. Both mouse BAR116 and mouse
915 *CS9* showed no enhancer activity in limbs[6,17], whereas the bat BAR116 displayed
916 different patterns between mouse fore- and hindlimb[6]. The sequences of both the bat
917 BAR116 (Myoluc2, GL429772: 6,606,808-6,608,652) and the chick *CS93* (galGal5,
918 chr7:16,104,952-16,105,803) were aligned onto the mouse genome. (B) Coordinates of
919 either the chick *CS93* (green rectangle), or the 2kb large region used for enhancer assay
920 (blue domain). The 2kb sequence contains the chick *CS93* region and the region of high
921 interactions with the *Hoxd10* to *Hoxd11* region in proximal wing bud cells at HH30.
922 Conservation plot of mouse *CS93* and bat BAR116 using the 2kb region of chick *CS93*
923 as a reference. The peaks represent a conservation higher than 50%. Pink regions are
924 conserved non-coding sequences. The phylogenetic tree shows the highest conservation

925 of the chick CS93 with the bat BAR116 sequences. (C) Enhancer activities of mouse
926 *CS93* and chick *CS93* in mouse fore- and hindlimb buds from E10.5 to E12.5. The *lacZ*
927 expression pattern (left) showed that mouse *CS93* has an enhancer activity in the proximal
928 region of developing limb buds at E10.5 to E12.5. In contrast to the mouse, the chick
929 *CS93* (right) showed differential enhancer activity between fore- and hindlimb buds at
930 E12.5, as was also reported for the bat BAR116 sequence. The numbers of *lacZ* positive
931 embryos over total transgene integrated are indicated.
932
933 **Fig. 4. Premature termination of T-DOM activity in chick leg buds.** (A, B)
934 Comparison of H3K27ac and H3K27me3 ChIP-seq profiles in either whole, proximal or
935 distal wing- and leg buds at HH19 (equivalent to mouse E9.5), HH20 (equivalent to
936 mouse E10) and HH28. (A) In chick leg bud, enrichment of H3K27ac at region '*a*' in T-
937 DOM was initially detected at HH19, whereas it was significantly decreased at HH20.
938 Few H3K27ac marks were scored in region '*b*' in hindlimb bud at both HH19 and HH20,
939 as compared with those in wing buds. At HH28, the accumulation of H3K27ac marks
940 was quite low in both the *HoxD* cluster and the T-DOM region in proximal leg, when
941 compared to distal wing cells, whereas the profiles of H3K27ac in the distal region where
942 *Hoxd* genes are strongly expressed were similar between wing and leg buds at HH28. (B)
943 In whole wing- and leg buds at HH20, several C-DOM regions were covered by
944 H3K27me3, whereas T-DOM was either not yet labelled, or started to be enriched around
945 *CS39* in forelimb bud and hindlimb buds, respectively. In proximal leg buds where *Hoxd*
946 expression was reduced, H3K27me3 enrichment was observed at the *HoxD* cluster and

947 over T-DOM, when compared to proximal forelimb buds. Both regions '*a*' and '*b*' in T-
948 DOM seemed to be specific targets of H3K27me3 enrichment. Enrichment (*Y-axis*) of
949 ChIP is shown as the $\log_2$ ratio of the normalized number of reads between ChIP and
950 input samples. FL, forelimb; HL, hindlimb.
951
952 **Fig. 5. Subtraction of CHi-C matrices between wing- and leg buds with plotted TADs.**
953 (A) The black lines demarcate the TADs in wing- and leg buds as identified using the
954 TopDom algorithm. Subtraction are those of CHi-C matrices shown in S5A and S5B Fig,
955 with wing bud cells in red and leg bud cells in blue. (B) Subtraction of the CHi-C matrices
956 shown in S5A and S5B Fig at regions between the *HoxD* cluster and the area ranging
957 from region *'a'* to region *'b'* within T-DOM, with a 5kb resolution. A significant decrease
958 in contacts was detected between the *HoxD* cluster and the *CS93* region, which
959 corresponded to the reduction in H3K27ac levels (black rectangle). The increased
960 contacts involving the *HoxD* cluster shown in red and blue represent wing- and leg buds
961 cells, respectively. ChIP-seq profiles of CTCF and H3K27ac from wing- and leg buds at
962 HH20 are shown in red and blue, respectively. Opened and closed arrowheads indicate
963 the orientation of the CTCF motives. Enrichments (*Y*-axis) of CTCF and H3K27ac ChIP
964 are shown at the normalized 1x sequencing depth or the $\log_2$ ratio of the normalized
965 number of reads between ChIP and input samples, respectively. FL, forelimb; HL,
966 hindlimb.
967
968 **Fig. 6. Leg bud-specific early activation of the chick *Hoxa13*.** (A) Expression patterns

969 and levels of *Hoxa13* and *Hoxd11* in chick wing- and leg buds from HH20 to HH22.
970 Stronger expression of *Hoxa13* was observed in chick leg bud as compared to that in wing
971 bud (top). Expression level of *Hoxd11* increased in wing bud as development proceeded,
972 yet it decreased in leg bud (bottom). Expression levels were normalized to *Gapdh* and
973 depicted as fold change relative to wing bud at HH20-21. Error bars indicate standard
974 deviation of three biological replicates. **P<0.01, Student's *t*-test. (B) Expression of
975 *Hoxa13* and *Hoxd11* in mouse fore- and hindlimb buds, from E10.5 to E10.75. Both genes
976 were increasingly transcribed in fore- and hindlimb buds as development proceeded.
977 Expression levels were normalized to *Gapdh* and depicted as fold change relative to
978 forelimb buds at E10.5. Error bars indicate standard deviation of two or four biological
979 replicates. **P<0.01, NS, P>0.05, Student's *t*-test.
980
981 **Fig. 7. Different effects of a T-DOM deletion on fore- and hindlimb buds.** (A) The
982 $HoxD^{Del(attp\text{-}SB3)}$ and $HoxD^{Del(Mtx\text{-}Ttn)}$ alleles were constructed by deleting T-DOM through
983 a ca. 1Mb or 2.1Mb large deletion, respectively (left, dashed line). *Hoxd11* expression in
984 E12.5 fore- and hindlimbs from either control ($HoxD^{Del(8\text{-}13)/+}$) animals (indicated as
985 '+/Δ') or mutants ($HoxD^{Del(attp\text{-}SB3)/Del(8\text{-}13)}$, $HoxD^{Del(Mtx\text{-}Ttn)/Del(8\text{-}13)}$, $HoxD^{Del(8\text{-}13)/+}$;$HoxC^{-/-}$,
986 $HoxD^{Del(attp\text{-}SB3)/Del(8\text{-}13)}$;$HoxC^{-/-}$) littermates (indicated as '*Del(attp-SB3)/Δ*', '*Del(Mtx-*
987 *Ttn)/Δ*', '+/Δ/$HoxC^{-/-}$', '*Del(attp-SB3)/Δ*/$HoxC^{-/-}$'). In *Del(attp-SB3)/Δ* mutant, *Hoxd11*
988 expression was dramatically reduced in proximal forelimbs (arrowhead). Unexpectedly
989 however, expression remained robust in proximal hindlimbs (arrowhead). In $HoxD^{Del(Mtx\text{-}}$
990 $^{TiE2)}$ mutant, *Hoxd11* expression disappeared in both proximal fore- and hindlimb buds

991 (arrowhead). The absence of both T-DOM and the *HoxC* cluster did not affect *Hoxd11*
992 expression. (B) HiC data adapted from ref[19] showing the two TADs on either side of
993 the *HoxD* cluster and the TAD next to T-DOM. 4C profiles represent contacts established
994 by *Hoxd11* in proximal fore- and hindlimb buds, from control or *Del(attp-SB3)/*Δ mutant
995 animals. In mutant cells deleted for T-DOM, (tracks 2 and 4), ectopic contacts between
996 *Hoxd11* and regions in the neighboring TAD appeared due to their new proximity to
997 *HoxD*. The shaded region with red arrows shows the domains where more contacts were
998 detected in mutant proximal hindlimb versus proximal forelimb buds. (C) Enlargement
999 of 4C profiles dispatched in (B), DNaseI, hyper-sensitive profiles using E11.5 embryos
1000 and potential limb enhancer regions (pink rectangles), as identified by using Limb-
1001 Enhancer Genie tool. Potential hindlimb-specific enhancers (HE) are shown by red
1002 arrows. (D) Mouse HE1 is active in the proximal fore- and hindlimb buds and in the trunk
1003 at E12.5. The number indicate stained embryos over total number of integrations. PFL,
1004 proximal forelimb; PHL, proximal hindlimb; HL, hindlimb.
1005
1006 **Fig. 8. TAD boundaries at the mouse and chicken *HoxD* cluster and effect of T-DOM**
1007 **deletion.** (A, B) TADs boundaries at the *HoxD* locus in mouse (A) and chick (B) limb
1008 buds. (A) In the mouse, the boundary moves along a few genes, in a window likely
1009 determined by a series of CTCF sites. In chick, the boundary appears less robust and
1010 slightly expanded towards the *Hoxd13* locus. This latter situation may enable T-DOM
1011 enhancers to interact with *Hoxd13* more efficiently in chick than in murine cells (B).
1012 Black and white arrowheads indicate the orientation of CTCF motives. (C) The different

1013 effects of T-DOM deletion in mouse proximal fore- and hindlimb cells. The
1014 transcriptional status of *Hoxd* genes is different between forelimb and hindlimb buds due
1015 to their prior expression or non-expression in lateral plate mesoderm, respectively. In the
1016 absence of T-DOM, H3K27me3 marks may accumulate over the silenced *Hoxd* genes in
1017 mutant forelimb buds as described in [17], making them poorly responsive to the HE1
1018 enhancer. In contrast, mutant hindlimb bud proximal cells have their *Hoxd* genes poised
1019 for activation and *de novo* interactions with the HE1 enhancer may occur. H3K27me3
1020 marks are in blue and presumptive factors, such as a potential mediator of DNA looping
1021 and a hindlimb-specific transcription factor, are shown by a green oval and a yellow star.
1022

1023 **SUPPORTING INFORMATION**

1024 **S1 Fig (related to Fig 1). *Hoxa* genes expression in mouse and chick limb buds.**

1025 **S2 Fig (related to Fig 2). The regulatory switch between TADs in mouse and chick**
1026 **limb buds.**

1027 **S3 Fig (related to Fig 4). H3K27ac, H3K27me3 and RNA-seq at *HoxD* in chick limbs.**

1028 **S4 Fig (related to Fig 4). H3K27ac and H3K27me3 profiles of ChIP-seq and RNA-**
1029 **seq at the *HoxA* locus in chick limbs.**

1030 **S5 Fig (related to Fig 5). Chromatin conformation at the chick *HoxD* locus in wing-**
1031 **and leg buds and conservation of CTCF sites orientations.**

1032 **S6 Fig (related to Fig 6). Expression of *Hoxa* and *Hoxd* genes in chick and mouse**
1033 **limb buds.**

1034 **S7 Fig (related to Fig 7). A T-DOM deletion induces interactions between HE1 and**

1035 ***Hoxd* genes.**

1036 **S1 Table. Information about samples.**

1037 **S2 Table. DNA sequences of primers used for both RT-qPCR analyses and**

1038 **genotyping.**

1039 **S3 Table. DNA sequences of primers used for 4C analyses.**

1040 Custom barcodes (4bp shown by NNNN) were introduced in between the Illumina

1041 adapter sequence and the specific viewpoint sequences to do multiplexing using different

1042 samples with the same viewpoint.

1043 **S4 Table. Public datasets used in this research.**

1044

1045 **References**

1046 1. Zeller R, Lopez-Rios J, Zuniga A. Vertebrate limb bud development: moving
1047 towards integrative analysis of organogenesis. Nature reviews Genetics. 2009;10: 845–
1048 58. doi:10.1038/nrg2681
1049 2. Blanco MJ, Misof BY, Wagner GP. Heterochronic differences of Hoxa-11
1050 expression in Xenopus fore- and hind limb development: evidence for lower limb identity
1051 of the anuran ankle bones. Dev Genes Evol. 1998;208: 175–87.
1052 3. Noro M, Uejima A, Abe G, Manabe M, Tamura K. Normal developmental stages
1053 of the Madagascar ground gecko Paroedura pictus with special reference to limb
1054 morphogenesis. Dev Dyn. 2009;238: 100–109. doi:10.1002/dvdy.21828
1055 4. Sears KE, Behringer RR, Rasweiler JJ, Niswander LA. Development of bat
1056 flight: morphologic and molecular evolution of bat wing digits. Proc Natl Acad Sci USA.
1057 2006;103: 6581–6586. doi:10.1073/pnas.0509716103
1058 5. Seki R, Kamiyama N, Tadokoro A, Nomura N, Tsuihiji T, Manabe M, et al.
1059 Evolutionary and developmental aspects of avian-specific traits in limb skeletal pattern.
1060 Zoolog Sci. 2012;29: 631–44. doi:10.2108/zsj.29.631
1061 6. Booker BM, Friedrich T, Mason MK, VanderMeer JE, Zhao J, Eckalbar WL, et

1062 al. Bat Accelerated Regions Identify a Bat Forelimb Specific Enhancer in the HoxD
1063 Locus. PLoS Genet. 2016;12: e1005738. doi:10.1371/journal.pgen.1005738
1064 7. Seki R, Li C, Fang Q, Hayashi S, Egawa S, Hu J, et al. Functional roles of Aves
1065 class-specific cis-regulatory elements on macroevolution of bird-specific features. Nat
1066 Commun. 2017;8: 14229. doi:10.1038/ncomms14229
1067 8. Domyan ET, Kronenberg Z, Infante CR, Vickrey AI, Stringham SA, Bruders R,
1068 et al. Molecular shifts in limb identity underlie development of feathered feet in two
1069 domestic avian species. Elife. 2016;5: e12115. doi:10.7554/eLife.12115
1070 9. Mallo M. Reassessing the Role of Hox Genes during Vertebrate Development
1071 and Evolution. Trends Genet. 2018;34: 209–217. doi:10.1016/j.tig.2017.11.007
1072 10. Wellik DM. Hox patterning of the vertebrate axial skeleton. Dev Dyn. 2007;236:
1073 2454–2463. doi:10.1002/(ISSN)1097-0177
1074 11. Wellik DM, Capecchi MR. Hox10 and Hox11 genes are required to globally
1075 pattern the mammalian skeleton. Science. 2003;301: 363–7.
1076 doi:10.1126/science.1085672
1077 12. Zakany J, Duboule D. The role of Hox genes during vertebrate limb development.
1078 Current Opinion in Genetics & Development. 2007;17: 359–66.
1079 doi:10.1016/j.gde.2007.05.011
1080 13. Nora EP, Lajoie BR, Schulz EG, Giorgetti L, Okamoto I, Servant N, et al. Spatial
1081 partitioning of the regulatory landscape of the X-inactivation centre. Nature. 2012;485:
1082 381–5. doi:10.1038/nature11049
1083 14. Dixon JR, Selvaraj S, Yue F, Kim A, Li Y, Shen Y, et al. Topological domains
1084 in mammalian genomes identified by analysis of chromatin interactions. Nature.
1085 2012;485: 376–80. doi:10.1038/nature11082
1086 15. Sexton T, Yaffe E, Kenigsberg E, Bantignies F, Leblanc B, Hoichman M, et al.
1087 Three-dimensional folding and functional organization principles of the Drosophila
1088 genome. Cell. 2012;148: 458–72. doi:10.1016/j.cell.2012.01.010
1089 16. Berlivet S, Paquette D, Dumouchel A, Langlais D, Dostie J, Kmita M. Clustering
1090 of tissue-specific sub-TADs accompanies the regulation of HoxA genes in developing
1091 limbs. PLoS genetics. 2013;9: e1004018. doi:10.1371/journal.pgen.1004018
1092 17. Andrey G, Montavon T, Mascrez B, Gonzalez F, Noordermeer D, Leleu M, et
1093 al. A switch between topological domains underlies HoxD genes collinearity in mouse
1094 limbs. Science. 2013;340: 1234167. doi:10.1126/science.1234167

1095 18. Montavon T, Soshnikova N, Mascrez B, Joye E, Thevenet L, Splinter E, et al. A
1096 regulatory archipelago controls Hox genes transcription in digits. Cell. 2011;147: 1132–
1097 45. doi:10.1016/j.cell.2011.10.023
1098 19. Rodriguez-Carballo E, Lopez-Delisle L, Zhan Y, Fabre PJ, Beccari L, El-Idrissi
1099 I, et al. The HoxD cluster is a dynamic and resilient TAD boundary controlling the
1100 segregation of antagonistic regulatory landscapes. Genes Dev. 2017;31: 2264–2281.
1101 doi:10.1101/gad.307769.117
1102 20. Beccari L, Yakushiji-Kaminatsui N, Woltering JM, Necsulea A, Lonfat N,
1103 Rodriguez-Carballo E, et al. A role for HOX13 proteins in the regulatory switch between
1104 TADs at the HoxD locus. Genes Dev. 2016;30: 1172–86. doi:10.1101/gad.281055.116
1105 21. Woltering JM, Noordermeer D, Leleu M, Duboule D. Conservation and
1106 divergence of regulatory strategies at Hox Loci and the origin of tetrapod digits. PLoS
1107 Biol. 2014;12: e1001773. doi:10.1371/journal.pbio.1001773
1108 22. Guerreiro I, Gitto S, Novoa A, Codourey J, Nguyen Huynh TH, Gonzalez F, et
1109 al. Reorganisation of Hoxd regulatory landscapes during the evolution of a snake-like
1110 body plan. eLife. 2016;5. doi:10.7554/eLife.16087
1111 23. Kamiyama N, Seki R, Yokoyama H, Tamura K. Heterochronically early decline
1112 of Hox expression prior to cartilage formation in the avian hindlimb zeugopod. Dev
1113 Growth Differ. 2012;54: 619–32. doi:10.1111/j.1440-169X.2012.01359.x
1114 24. Flöttmann R, Kragesteen BK, Geuer S, Socha M, Allou L, Sowińska-Seidler A,
1115 et al. Noncoding copy-number variations are associated with congenital limb
1116 malformation. Genet Med. 2017; doi:10.1038/gim.2017.154
1117 25. Villavicencio-Lorini P, Kuss P, Friedrich J, Haupt J, Farooq M, Turkmen S, et
1118 al. Homeobox genes d11-d13 and a13 control mouse autopod cortical bone and joint
1119 formation. The Journal of clinical investigation. 2010;120: 1994–2004.
1120 doi:10.1172/JCI41554
1121 26. Yokouchi Y, Nakazato S, Yamamoto M, Goto Y, Kameda T, Iba H, et al.
1122 Misexpression of Hoxa-13 induces cartilage homeotic transformation and changes cell
1123 adhesiveness in chick limb buds. Genes & development. 1995;9: 2509–22.
1124 27. Tschopp P, Duboule D. A regulatory "landscape effect" over the HoxD cluster.
1125 Developmental biology. 2011;351: 288–96. doi:10.1016/j.ydbio.2010.12.034
1126 28. Spitz F, Montavon T, Monso-Hinard C, Morris M, Ventruto M-L, Antonarakis
1127 S, et al. A t(2;8) balanced translocation with breakpoints near the human HOXD complex

1128 causes mesomelic dysplasia and vertebral defects. Genomics. 2002;79: 493–8.
1129 doi:10.1006/geno.2002.6735
1130 29. Gonzalez-Martin MC, Mallo M, Ros MA. Long bone development requires a
1131 threshold of Hox function. Developmental biology. 2014;392: 454–65.
1132 doi:10.1016/j.ydbio.2014.06.004
1133 30. Herault Y, Fraudeau N, Zakany J, Duboule D. Ulnaless (Ul), a regulatory
1134 mutation inducing both loss-of-function and gain-of-function of posterior Hoxd genes.
1135 Development. 1997;124: 3493–500.
1136 31. Nelson CE, Morgan BA, Burke AC, Laufer E, DiMambro E, Murtaugh LC, et
1137 al. Analysis of Hox gene expression in the chick limb bud. Development. 1996;122:
1138 1449–66.
1139 32. Friedli M, Barde I, Arcangeli M, Verp S, Quazzola A, Zakany J, et al. A
1140 systematic enhancer screen using lentivector transgenesis identifies conserved and non-
1141 conserved functional elements at the Olig1 and Olig2 locus. PLoS ONE. 2010;5: e15741.
1142 doi:10.1371/journal.pone.0015741
1143 33. Lois C, Hong EJ, Pease S, Brown EJ, Baltimore D. Germline transmission and
1144 tissue-specific expression of transgenes delivered by lentiviral vectors. Science.
1145 2002;295: 868–72. doi:10.1126/science.1067081
1146 34. Martin P. Tissue patterning in the developing mouse limb. Int J Dev Biol.
1147 1990;34: 323–336.
1148 35. Fernández-Terán MA, Hinchliffe JR, Ros MA. Birth and death of cells in limb
1149 development: a mapping study. Dev Dyn. 2006;235: 2521–2537.
1150 doi:10.1002/dvdy.20916
1151 36. Tie F, Banerjee R, Stratton CA, Prasad-Sinha J, Stepanik V, Zlobin A, et al.
1152 CBP-mediated acetylation of histone H3 lysine 27 antagonizes Drosophila Polycomb
1153 silencing. Development. 2009;136: 3131–41. doi:10.1242/dev.037127
1154 37. Bonev B, Mendelson Cohen N, Szabo Q, Fritsch L, Papadopoulos GL, Lubling
1155 Y, et al. Multiscale 3D Genome Rewiring during Mouse Neural Development. Cell.
1156 2017;171: 557-572.e24. doi:10.1016/j.cell.2017.09.043
1157 38. Rao SS, Huntley MH, Durand NC, Stamenova EK, Bochkov ID, Robinson JT,
1158 et al. A 3D map of the human genome at kilobase resolution reveals principles of
1159 chromatin looping. Cell. 2014;159: 1665–80. doi:10.1016/j.cell.2014.11.021
1160 39. Deng W, Rupon JW, Krivega I, Breda L, Motta I, Jahn KS, et al. Reactivation

1161 of developmentally silenced globin genes by forced chromatin looping. Cell. 2014;158:
1162 849–860. doi:10.1016/j.cell.2014.05.050
1163 40. Dryden NH, Broome LR, Dudbridge F, Johnson N, Orr N, Schoenfelder S, et al.
1164 Unbiased analysis of potential targets of breast cancer susceptibility loci by Capture Hi-
1165 C. Genome Res. 2014;24: 1854–1868. doi:10.1101/gr.175034.114
1166 41. Hughes JR, Roberts N, McGowan S, Hay D, Giannoulatou E, Lynch M, et al.
1167 Analysis of hundreds of cis-regulatory landscapes at high resolution in a single, high-
1168 throughput experiment. Nat Genet. 2014;46: 205–212. doi:10.1038/ng.2871
1169 42. Shin H, Shi Y, Dai C, Tjong H, Gong K, Alber F, et al. TopDom: an efficient
1170 and deterministic method for identifying topological domains in genomes. Nucleic acids
1171 research. 2016;44: e70. doi:10.1093/nar/gkv1505
1172 43. Soshnikova N, Montavon T, Leleu M, Galjart N, Duboule D. Functional analysis
1173 of CTCF during mammalian limb development. Dev Cell. 2010;19: 819–30.
1174 doi:10.1016/j.devcel.2010.11.009
1175 44. Narendra V, Bulajić M, Dekker J, Mazzoni EO, Reinberg D. CTCF-mediated
1176 topological boundaries during development foster appropriate gene regulation. Genes
1177 Dev. 2016;30: 2657–2662. doi:10.1101/gad.288324.116
1178 45. Darbellay F, Duboule D. Topological Domains, Metagenes, and the Emergence
1179 of Pleiotropic Regulations at Hox Loci. Current topics in developmental biology.
1180 2016;116: 299–314. doi:10.1016/bs.ctdb.2015.11.022
1181 46. Merkenschlager M, Nora EP. CTCF and Cohesin in Genome Folding and
1182 Transcriptional Gene Regulation. Annual review of genomics and human genetics.
1183 2016;17: 17–43. doi:10.1146/annurev-genom-083115-022339
1184 47. Sanborn AL, Rao SSP, Huang S-C, Durand NC, Huntley MH, Jewett AI, et al.
1185 Chromatin extrusion explains key features of loop and domain formation in wild-type and
1186 engineered genomes. Proc Natl Acad Sci USA. 2015;112: E6456-6465.
1187 doi:10.1073/pnas.1518552112
1188 48. Andrey G, Schöpflin R, Jerković I, Heinrich V, Ibrahim DM, Paliou C, et al.
1189 Characterization of hundreds of regulatory landscapes in developing limbs reveals two
1190 regimes of chromatin folding. Genome Res. 2017;27: 223–233.
1191 doi:10.1101/gr.213066.116
1192 49. Sheth R, Barozzi I, Langlais D, Osterwalder M, Nemec S, Carlson HL, et al.
1193 Distal Limb Patterning Requires Modulation of cis-Regulatory Activities by HOX13.

1194 Cell Rep. 2016;17: 2913–2926. doi:10.1016/j.celrep.2016.11.039
1195 50. Towers M, Tickle C. Growing models of vertebrate limb development.
1196 Development. 2009;136: 179–90. doi:10.1242/dev.024158
1197 51. Hamburger V, Hamilton HL. A series of normal stages in the development of
1198 the chick embryo. 1951. Developmental dynamics : an official publication of the
1199 American Association of Anatomists. 1992;195: 231–72. doi:10.1002/aja.1001950404
1200 52. Mercader N, Selleri L, Criado LM, Pallares P, Parras C, Cleary ML, et al.
1201 Ectopic Meis1 expression in the mouse limb bud alters P-D patterning in a Pbx1-
1202 independent manner. Int J Dev Biol. 2009;53: 1483–94. doi:10.1387/ijdb.072430nm
1203 53. ENCODE Project Consortium. An integrated encyclopedia of DNA elements in
1204 the human genome. Nature. 2012;489: 57–74. doi:10.1038/nature11247
1205 54. Monti R, Barozzi I, Osterwalder M, Lee E, Kato M, Garvin TH, et al. Limb-
1206 Enhancer Genie: An accessible resource of accurate enhancer predictions in the
1207 developing limb. PLoS Comput Biol. 2017;13: e1005720.
1208 doi:10.1371/journal.pcbi.1005720
1209 55. Peterson RL, Papenbrock T, Davda MM, Awgulewitsch A. The murine Hoxc
1210 cluster contains five neighboring AbdB-related Hox genes that show unique spatially
1211 coordinated expression in posterior embryonic subregions. Mech Dev. 1994;47: 253–60.
1212 56. Davis AP, Witte DP, Hsieh-Li HM, Potter SS, Capecchi MR. Absence of radius
1213 and ulna in mice lacking hoxa-11 and hoxd-11. Nature. 1995;375: 791–5.
1214 doi:10.1038/375791a0
1215 57. Suemori H, Noguchi S. Hox C cluster genes are dispensable for overall body
1216 plan of mouse embryonic development. Dev Biol. 2000;220: 333–42.
1217 doi:10.1006/dbio.2000.9651
1218 58. Carpenter EM, Goddard JM, Davis AP, Nguyen TP, Capecchi MR. Targeted
1219 disruption of Hoxd-10 affects mouse hindlimb development. Development. 1997;124:
1220 4505–14.
1221 59. Rodrigues AR, Tabin CJ. Developmental biology. Deserts and waves in gene
1222 expression. Science. 2013;340: 1181–2. doi:10.1126/science.1239867
1223 60. Itzkovitz B, Jiralerspong S, Nimmo G, Loscalzo M, Horovitz DDG, Snowden
1224 A, et al. Functional characterization of novel mutations in GNPAT and AGPS, causing
1225 rhizomelic chondrodysplasia punctata (RCDP) types 2 and 3. Hum Mutat. 2012;33: 189–
1226 197. doi:10.1002/humu.21623

1227 61. Liegel RP, Ronchetti A, Sidjanin DJ. Alkylglycerone phosphate synthase
1228 (AGPS) deficient mice: models for rhizomelic chondrodysplasia punctate type 3
1229 (RCDP3) malformation syndrome. Mol Genet Metab Rep. 2014;1: 299–311.
1230 doi:10.1016/j.ymgmr.2014.06.003
1231 62. Weintraub AS, Li CH, Zamudio AV, Sigova AA, Hannett NM, Day DS, et al.
1232 YY1 Is a Structural Regulator of Enhancer-Promoter Loops. Cell. 2017;171: 1573-
1233 1588.e28. doi:10.1016/j.cell.2017.11.008
1234 63. Infante CR, Park S, Mihala AG, Kingsley DM, Menke DB. Pitx1 broadly
1235 associates with limb enhancers and is enriched on hindlimb cis-regulatory elements. Dev
1236 Biol. 2013;374: 234–244. doi:10.1016/j.ydbio.2012.11.017
1237 64. Woltering JM, Vonk FJ, Muller H, Bardine N, Tuduce IL, de Bakker MA, et al.
1238 Axial patterning in snakes and caecilians: evidence for an alternative interpretation of the
1239 Hox code. Developmental biology. 2009;332: 82–9. doi:10.1016/j.ydbio.2009.04.031
1240 65. Kim D, Pertea G, Trapnell C, Pimentel H, Kelley R, Salzberg SL. TopHat2:
1241 accurate alignment of transcriptomes in the presence of insertions, deletions and gene
1242 fusions. Genome biology. 2013;14: R36. doi:10.1186/gb-2013-14-4-r36
1243 66. Li H, Handsaker B, Wysoker A, Fennell T, Ruan J, Homer N, et al. The Sequence
1244 Alignment/Map format and SAMtools. Bioinformatics. 2009;25: 2078–9.
1245 doi:10.1093/bioinformatics/btp352
1246 67. Afgan E, Baker D, van den Beek M, Blankenberg D, Bouvier D, Čech M, et al.
1247 The Galaxy platform for accessible, reproducible and collaborative biomedical analyses:
1248 2016 update. Nucleic Acids Res. 2016;44: W3–W10. doi:10.1093/nar/gkw343
1249 68. Noordermeer D, Leleu M, Schorderet P, Joye E, Chabaud F, Duboule D.
1250 Temporal dynamics and developmental memory of 3D chromatin architecture at Hox
1251 gene loci. eLife. 2014;3: e02557. doi:10.7554/eLife.02557
1252 69. Noordermeer D, Leleu M, Splinter E, Rougemont J, De Laat W, Duboule D. The
1253 dynamic architecture of Hox gene clusters. Science. 2011;334: 222–5.
1254 doi:10.1126/science.1207194
1255 70. David FP, Delafontaine J, Carat S, Ross FJ, Lefebvre G, Jarosz Y, et al.
1256 HTSstation: a web application and open-access libraries for high-throughput sequencing
1257 data analysis. PloS one. 2014;9: e85879. doi:10.1371/journal.pone.0085879
1258 71. Langmead B, Trapnell C, Pop M, Salzberg SL. Ultrafast and memory-efficient
1259 alignment of short DNA sequences to the human genome. Genome biology. 2009;10:

1260 R25. doi:10.1186/gb-2009-10-3-r25
1261 72. Riising EM, Comet I, Leblanc B, Wu X, Johansen JV, Helin K. Gene silencing
1262 triggers polycomb repressive complex 2 recruitment to CpG islands genome wide.
1263 Molecular cell. 2014;55: 347–60. doi:10.1016/j.molcel.2014.06.005
1264 73. Ramirez F, Dundar F, Diehl S, Gruning BA, Manke T. deepTools: a flexible
1265 platform for exploring deep-sequencing data. Nucleic acids research. 2014;42: W187-91.
1266 doi:10.1093/nar/gku365
1267 74. Ramirez F, Ryan DP, Gruning B, Bhardwaj V, Kilpert F, Richter AS, et al.
1268 deepTools2: a next generation web server for deep-sequencing data analysis. Nucleic
1269 acids research. 2016;44: W160-5. doi:10.1093/nar/gkw257
1270 75. Belaghzal H, Dekker J, Gibcus JH. Hi-C 2.0: An optimized Hi-C procedure for
1271 high-resolution genome-wide mapping of chromosome conformation. Methods.
1272 2017;123: 56–65. doi:10.1016/j.ymeth.2017.04.004
1273 76. Martin M. Cutadapt removes adapter sequences from high-throughput
1274 sequencing reads. 2011. 2011;17. doi:10.14806/ej.17.1.200
1275 77. Langmead B, Salzberg SL. Fast gapped-read alignment with Bowtie 2. Nat
1276 Methods. 2012;9: 357–9. doi:10.1038/nmeth.1923
1277 78. Tarchini B, Huynh TH, Cox GA, Duboule D. HoxD cluster scanning deletions
1278 identify multiple defects leading to paralysis in the mouse mutant Ironside. Genes &
1279 development. 2005;19: 2862–76. doi:10.1101/gad.351105
1280 79. Radke MH, Peng J, Wu Y, McNabb M, Nelson OL, Granzier H, et al. Targeted
1281 deletion of titin N2B region leads to diastolic dysfunction and cardiac atrophy. Proc Natl
1282 Acad Sci USA. 2007;104: 3444–3449. doi:10.1073/pnas.0608543104

1283

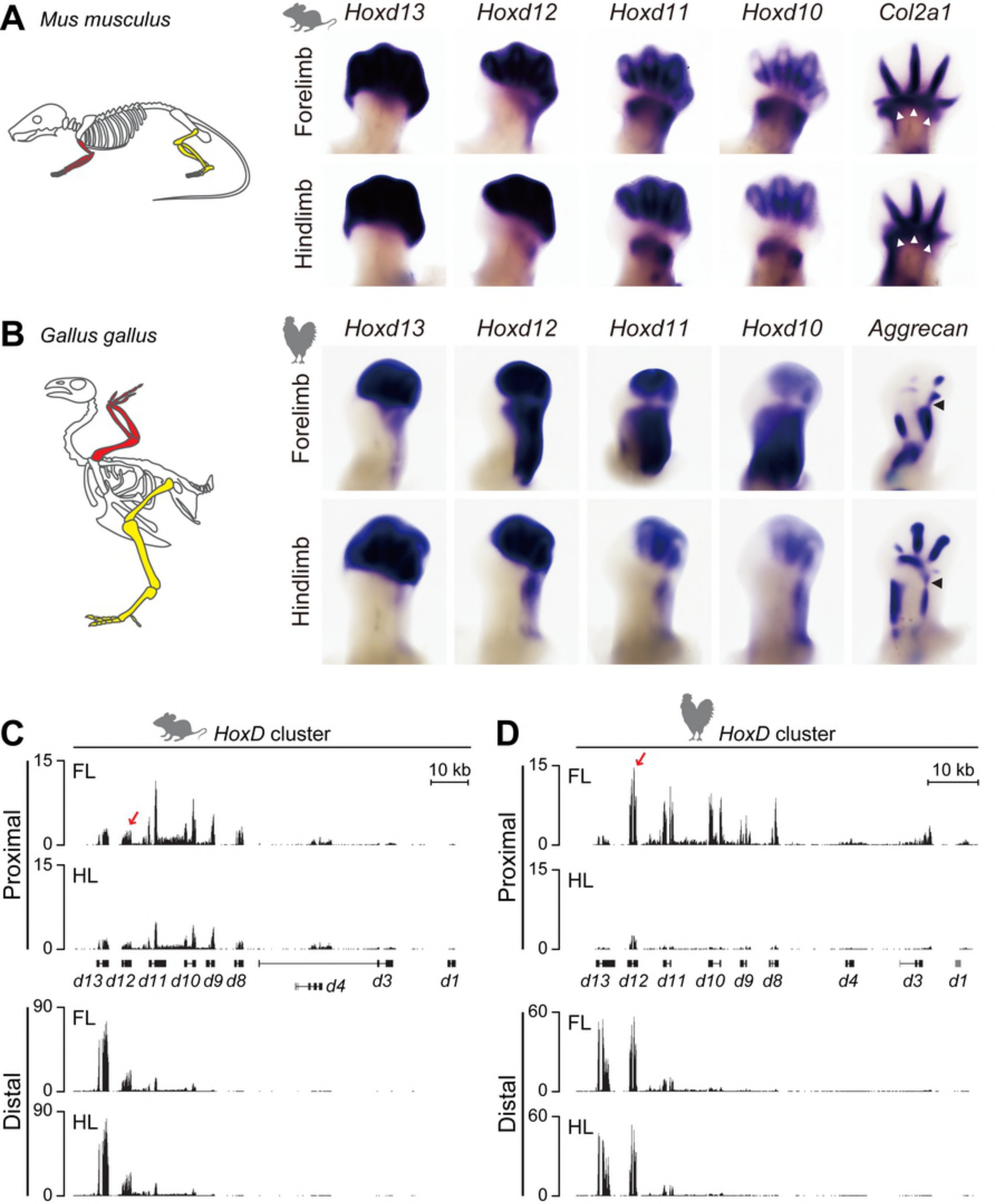
A
Mus musculus
Hoxd13
Hoxd12
Hoxd11
Hoxd10
Col2a1
Forelimb
Hindlimb
B
Gallus gallus
Hoxd13
Hoxd12
Hoxd11
Hoxd10
Aggrecan
Forelimb
Hindlimb
C
HoxD cluster
Proximal
Distal
FL
HL
10 kb
15
0
90
d13 d12 d11 d10 d9 d8
d4
d3
d1
D
HoxD cluster
Proximal
Distal
FL
HL
10 kb
15
0
60
d13 d12 d11 d10 d9 d8
d4
d3
d1

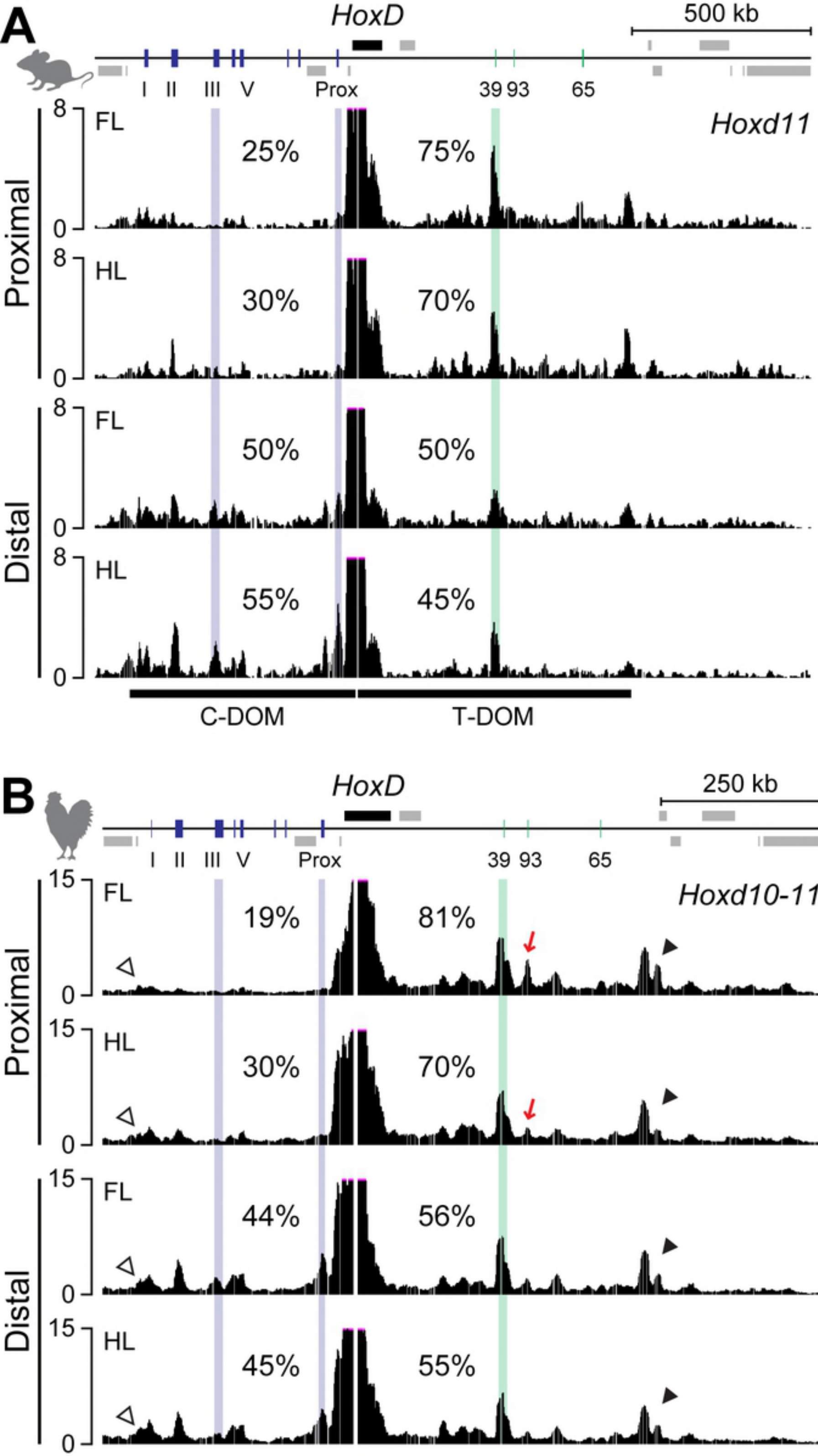
A
HoxD
500 kb
I
II
III
V
Prox
39
93
65
Hoxd11
Proximal
Distal
FL
HL
8
0
25%
75%
30%
70%
50%
50%
55%
45%
C-DOM
T-DOM
B
HoxD
250 kb
Hoxd10-11
15
19%
81%
30%
70%
44%
56%
45%
55%

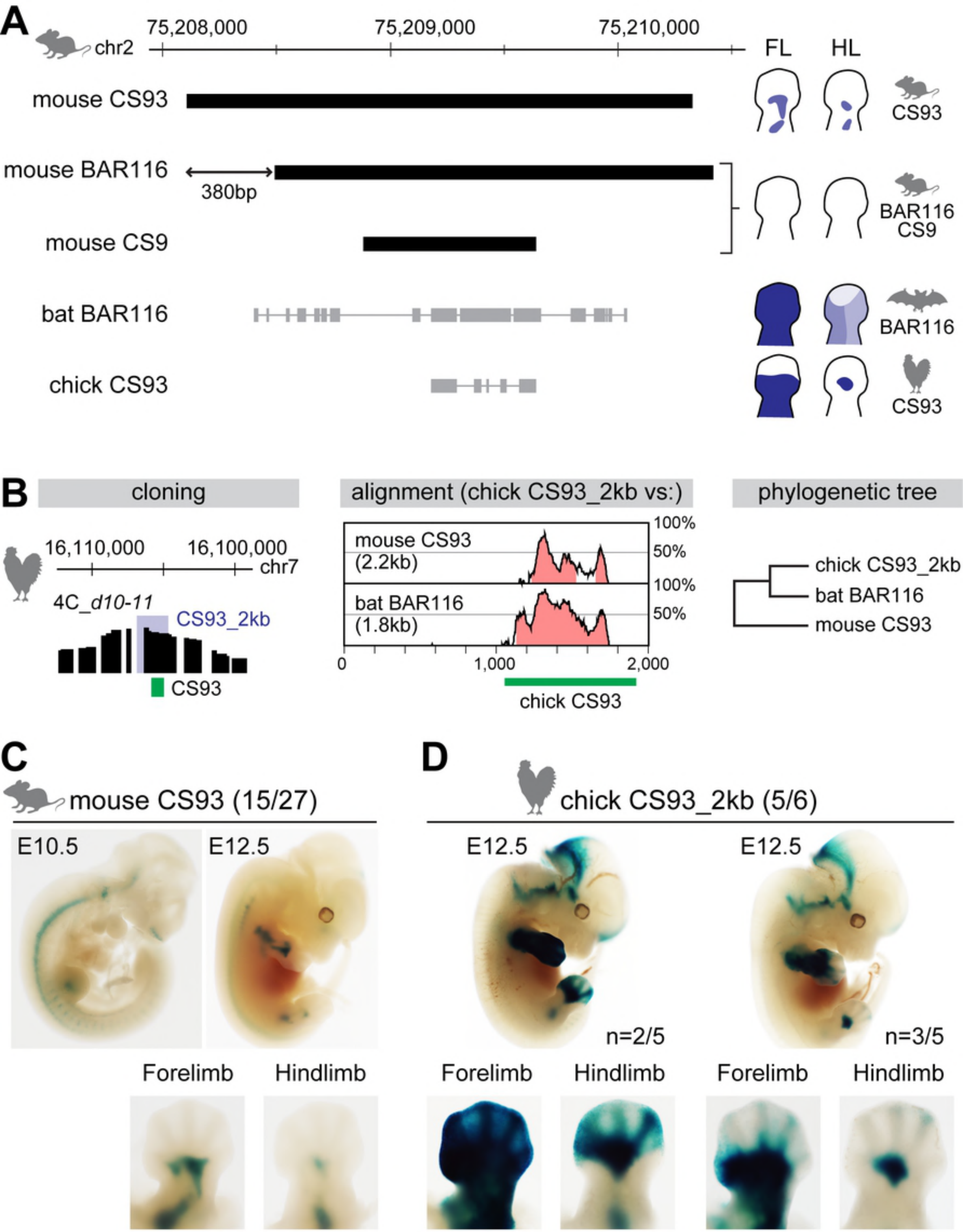
A
chr2
75,208,000
75,209,000
75,210,000
FL
HL
mouse CS93
CS93
mouse BAR116
380bp
mouse CS9
BAR116
CS9
bat BAR116
BAR116
chick CS93
CS93
B
cloning
16,110,000
16,100,000
chr7
4C_d10-11
CS93_2kb
CS93
alignment (chick CS93_2kb vs:)
mouse CS93
(2.2kb)
bat BAR116
(1.8kb)
100%
50%
100%
50%
0
1,000
2,000
chick CS93
phylogenetic tree
chick CS93_2kb
bat BAR116
mouse CS93
C
mouse CS93 (15/27)
E10.5
E12.5
D
chick CS93_2kb (5/6)
E12.5
E12.5
n=2/5
n=3/5
Forelimb
Hindlimb
Forelimb
Hindlimb
Forelimb
Hindlimb

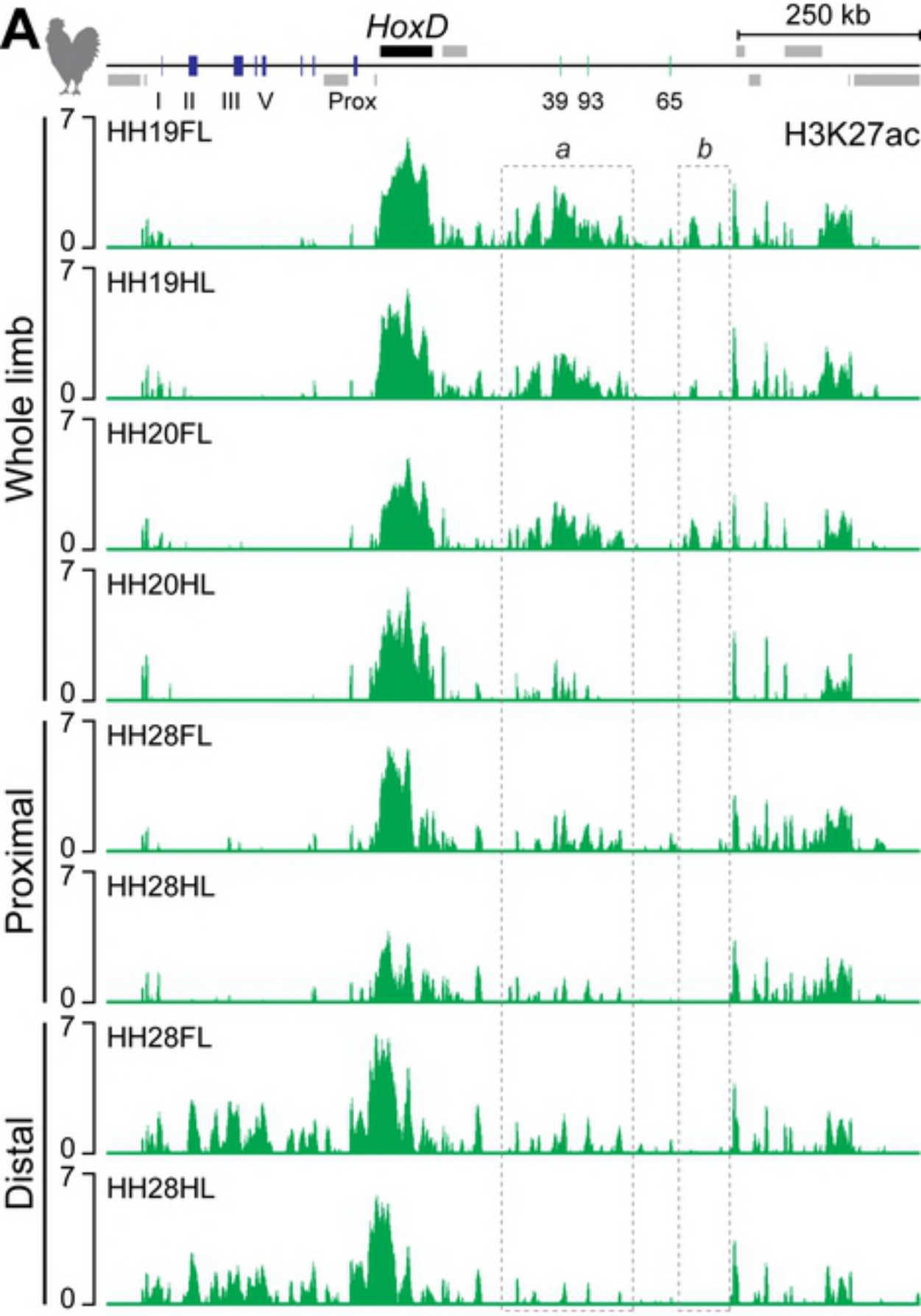
A
HoxD
250 kb
I II III V
Prox
39 93
65
H3K27ac
a
b
HH19FL
HH19HL
HH20FL
HH20HL
HH28FL
HH28HL
HH28FL
HH28HL
Whole limb
Proximal
Distal
7
0

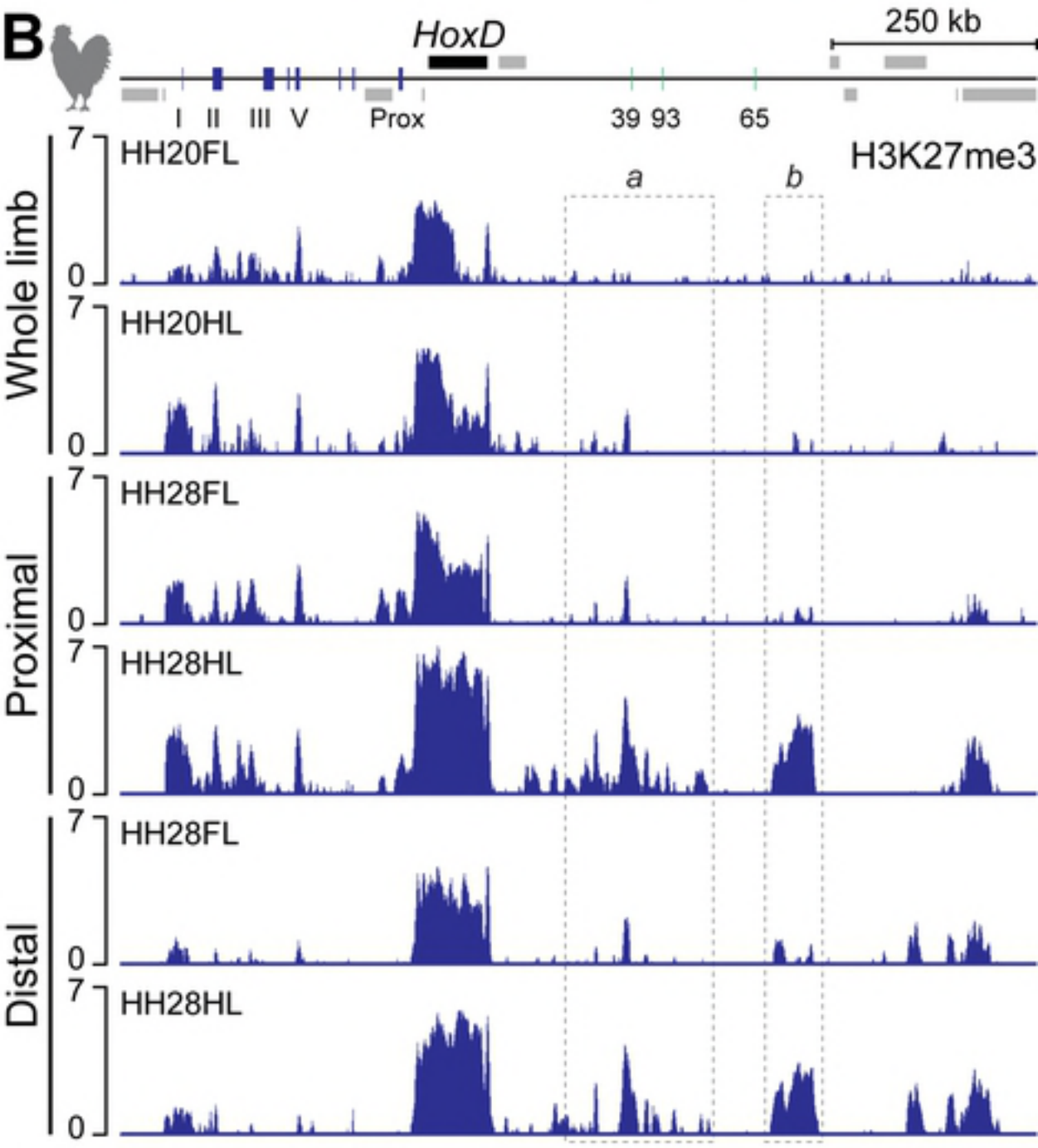
B
HoxD
250 kb
I II III V
Prox
39 93
65
H3K27me3
a
b
HH20FL
HH20HL
HH28FL
HH28HL
HH28FL
HH28HL
Whole limb
Proximal
Distal
7
0

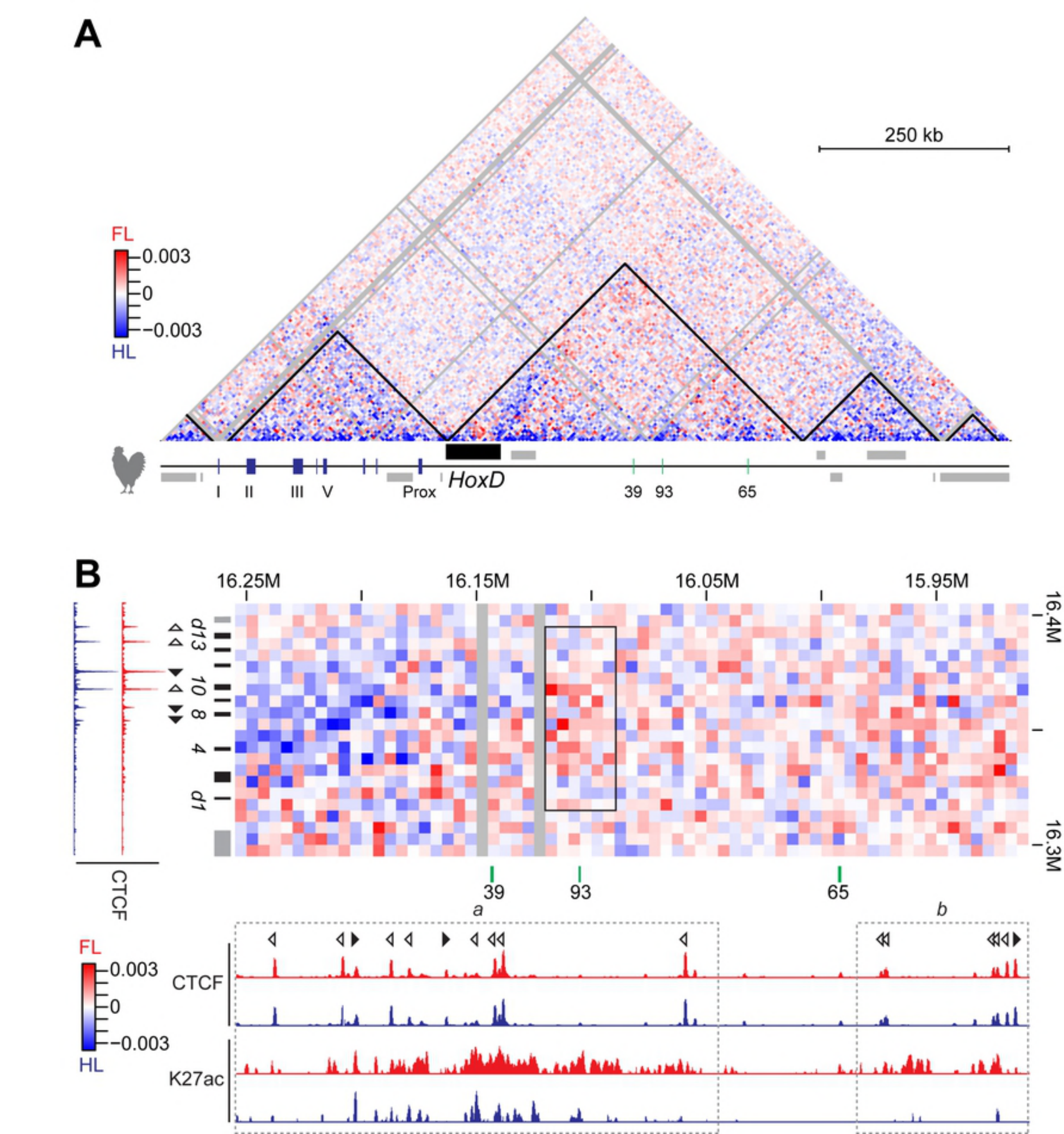
A
250 kb
FL
0.003
0
−0.003
HL
I
II
III
V
Prox
HoxD
39
93
65
B
16.25M
16.15M
16.05M
15.95M
16.4M
16.3M
d13
10
8
4
d1
CTCF
39
93
65
a
b
FL
0.003
0
−0.003
HL
CTCF
K27ac

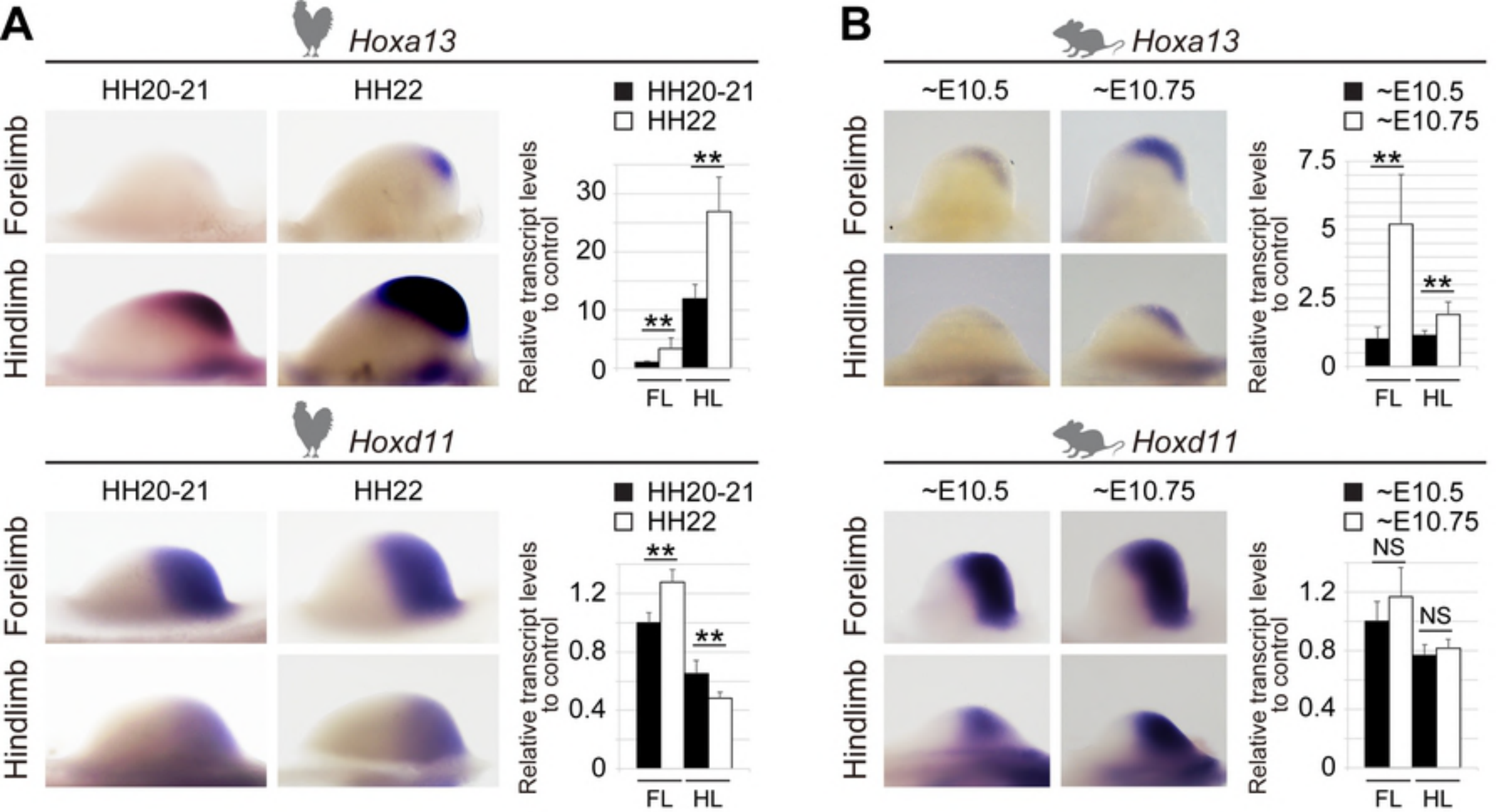
A
Hoxa13
HH20-21
HH22
Forelimb
Hindlimb
HH20-21
HH22
Relative transcript levels to control
30
20
10
0
**
**
FL
HL
Hoxd11
HH20-21
HH22
Forelimb
Hindlimb
HH20-21
HH22
Relative transcript levels to control
1.2
0.8
0.4
0
**
**
FL
HL
B
Hoxa13
~E10.5
~E10.75
Forelimb
Hindlimb
~E10.5
~E10.75
Relative transcript levels to control
7.5
5
2.5
0
**
**
FL
HL
Hoxd11
~E10.5
~E10.75
Forelimb
Hindlimb
~E10.5
~E10.75
Relative transcript levels to control
1.2
0.8
0.4
0
NS
NS
FL
HL

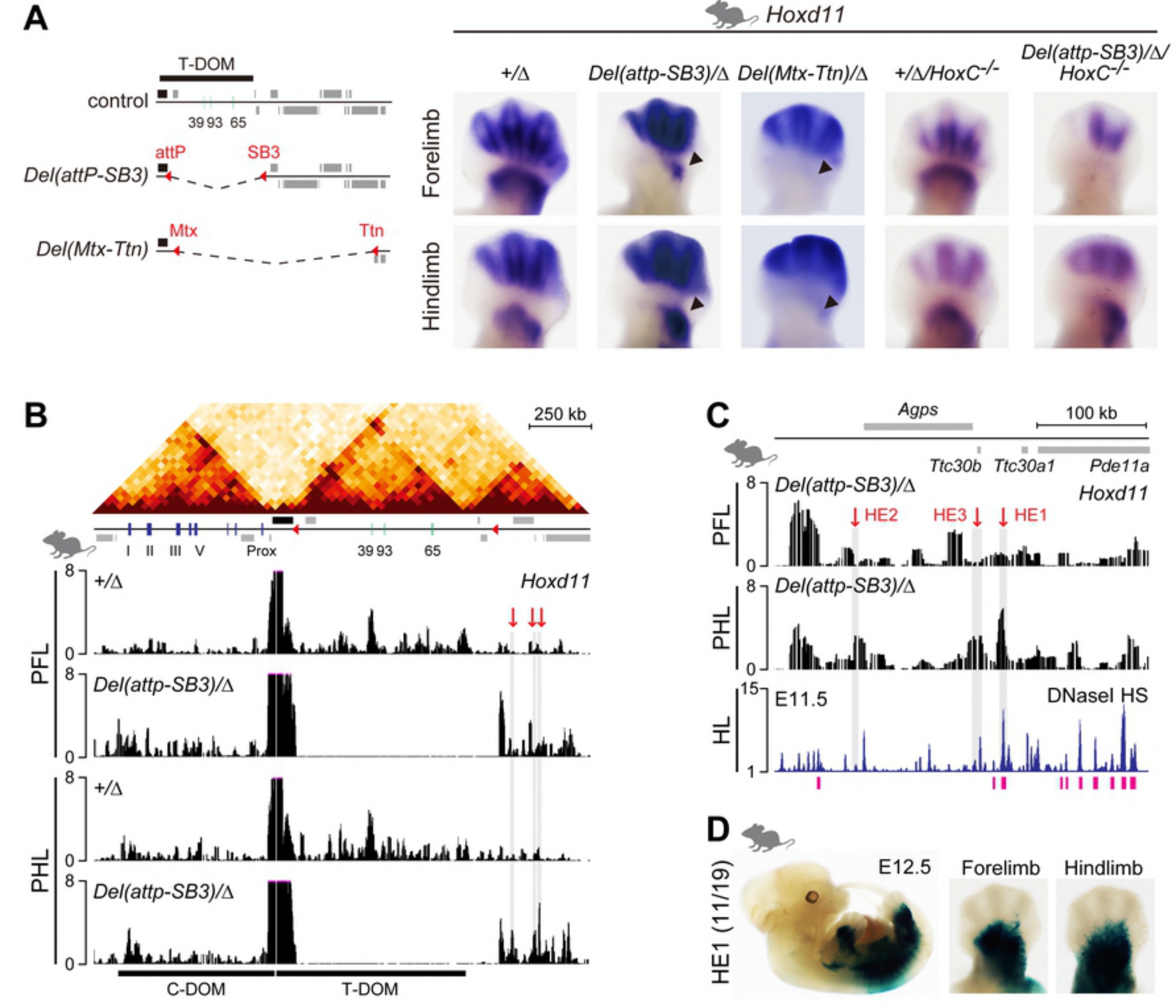
A
Hoxd11
T-DOM
control
39 93 65
attP
SB3
Del(attP-SB3)
Mtx
Ttn
Del(Mtx-Ttn)
+/Δ
Del(attp-SB3)/Δ
Del(Mtx-Ttn)/Δ
+/Δ/HoxC-/-
Del(attp-SB3)/Δ/HoxC-/-
Forelimb
Hindlimb
B
250 kb
I II III V
Prox
39 93
65
+/Δ
Hoxd11
Del(attp-SB3)/Δ
PFL
PHL
C-DOM
T-DOM
C
Agps
100 kb
Ttc30b
Ttc30a1
Pde11a
Hoxd11
Del(attp-SB3)/Δ
HE2
HE3
HE1
PFL
PHL
HL
E11.5
DNaseI HS
D
HE1 (11/19)
E12.5
Forelimb
Hindlimb

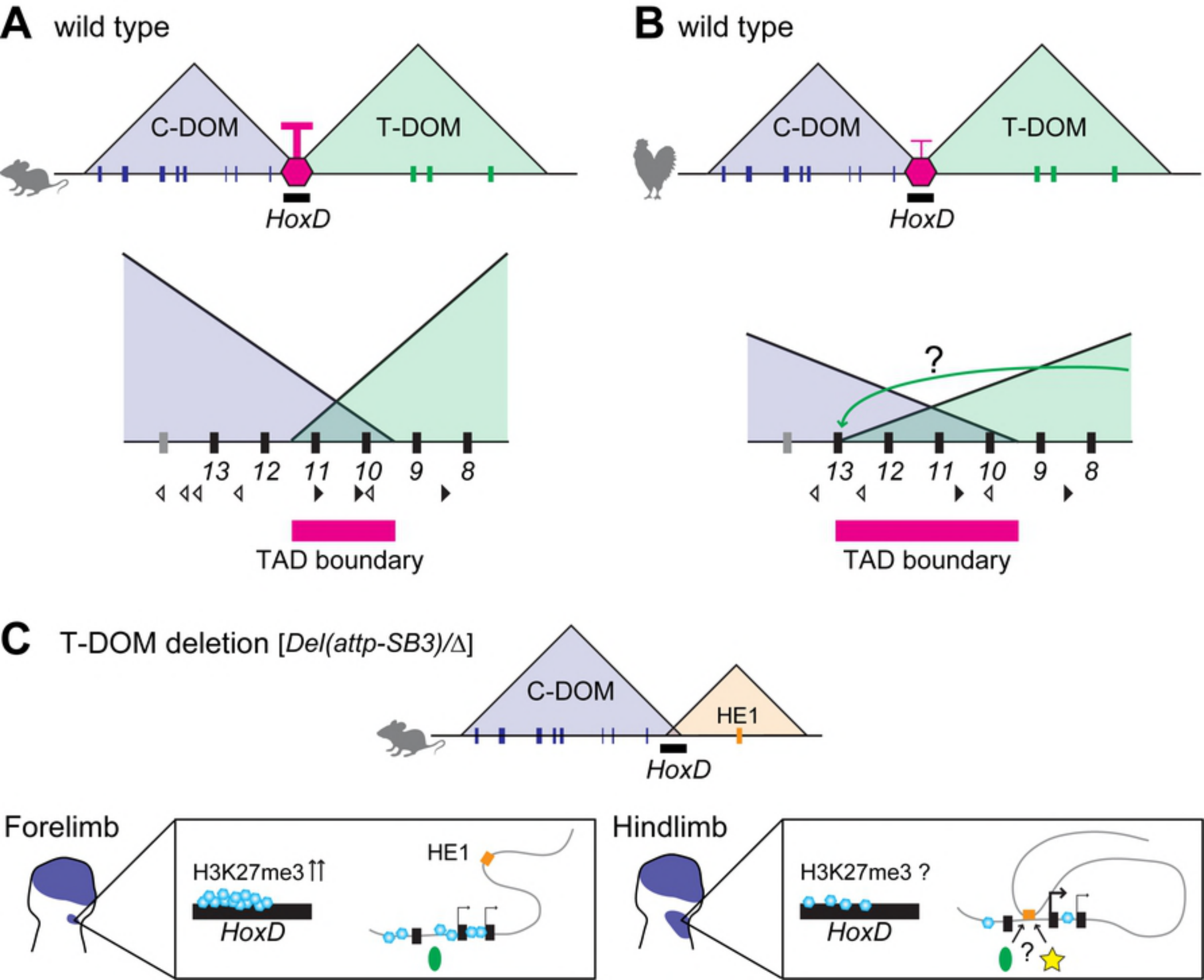
A wild type
C-DOM
T-DOM
HoxD
13 12 11 10 9 8
TAD boundary
B wild type
C-DOM
T-DOM
HoxD
?
13 12 11 10 9 8
TAD boundary
C T-DOM deletion [Del(attp-SB3)/Δ]
C-DOM
HE1
HoxD
Forelimb
H3K27me3 ↑↑
HoxD
HE1
Hindlimb
H3K27me3 ?
HoxD
?